https://doi.org/10.5194/egusphere-2024-2653
Preprint. Discussion started: 1 October 2024

EastGRIP ice core reveals the exceptional evolution of crystallographic preferred orientation throughout the Northeast Greenland Ice Stream

Nicolas Stoll[1,2,3], Ilka Weikusat[1,4], Daniela Jansen[1], Paul Bons[4], Kyra Darányi[1,4,5], Julien Westhoff[6], María-Gema Llorens[7], David Wallis[8], Jan Eichler[1,9], Tomotaka Saruya[10], Tomoyuki Homma[11], Martyn Drury[5], Frank Wilhelms[1,12], Sepp Kipfstuhl[1], Dorthe Dahl-Jensen[6,13], and Johanna Kerch[1,12]

[1]Department of Geosciences, Alfred Wegener Institute Helmholtz Centre for Polar and Marine Research, Bremerhaven, Germany
[2]Department of Environmental Sciences, Informatics and Statistics, Ca'Foscari University of Venice, Venice, Italy
[3]Department of Earth and Space Sciences, University of Washington, Seattle, USA
[4]Geoscience Department, Eberhard Karls University, Tübingen, Germany
[5]Department of Earth Sciences, Utrecht University, Utrecht, The Netherlands
[6]Physics of Ice, Climate and Earth, Niels Bohr Institute, University of Copenhagen, Copenhagen, Denmark
[7]GEO3BCN-CSIC, Lluís Solé Sabarís s/n, 08028 Barcelona, Spain
[8]Department of Earth Sciences, University of Cambridge, Cambridge, CB2 3EQ, UK
[9]Laboratoire de Géologie de Lyon: Terre, Planètes, Environnement (LGL-TPE), ENS Lyon, Université Claude Bernard Lyon 1, CNRS, Villeurbanne, France
[10]National Institute of Polar Research, Tokyo 190-8518, Japan
[11]Nagaoka University of Technology, 1603-1 Kamitomioka-machi, Nagaoka 940-2188, Japan
[12]Geoscience Centre, University of Göttingen, Göttingen, Germany
[13]Centre for Earth Observation Science, University of Manitoba, Winnipeg, Canada

Correspondence: Ilka Weikusat (ilka.weikusat@awi.de)

Abstract. A better understanding of glacial ice flow and how it is influenced by internal deformation is required to improve the projections of future sea-level rise in a warming climate. Especially large ice streams, the main contributors to solid ice discharge to the ocean, still require more observational data to be represented sufficiently in numerical ice-sheet models. The East Greenland Ice-core Project (EastGRIP) successfully drilled the first continuous deep ice core through an active ice stream, the Northeast Greenland Ice Stream (NEGIS), focusing on investigating the dynamical processes that lead to its exceptionally high velocity. Here, we show Crystallographic Preferred Orientations (CPO) data in 5–15 m depth resolution throughout 2663 m, down to bedrock, to determine the deformation regimes in this ice stream setting complemented by grain-size and borehole temperature profiles for context. A broad single-maximum CPO pattern is present in the upper 200 m caused by overlying snow and ice layers. Below, a crossed girdle CPO is observed for the first time in a deep ice core and we discuss possible formation mechanisms. Between 500 and 1230 m of depth, we observe a vertical girdle CPO indicative of along-flow extensional deformation. A complementary simple-shear component and polygonization explain the CPO between 1230 and 2500 m, a vertical girdle with horizontal maxima of varying strength. Close to bedrock, a multi-maxima CPO originates from migration recrystallisation due to high temperatures close to the pressure melting point. Ice at this depth is characterised by centimetre-large, amoeboid-shaped grains, which, together with the conductivity data from the deepest 260 m, indicates that

https://doi.org/10.5194/egusphere-2024-2653
Preprint. Discussion started: 1 October 2024

the core contains ice from the last Eemian. A comparison with other deep ice cores from Greenland and Antarctica shows the uniquely fast development of CPO at shallow depths in the EastGRIP ice core due to its location in an area of high strain rates while the grain-size evolution with depth remains similar to less dynamic sites confirming that it is mainly governed by the varying purity of ice deposited during varying climatic conditions. We further show that the overall plug flow of NEGIS is characterised by many small-scale variations, which remain to be considered in ice-flow models.

1 Introduction

Melting and solid ice discharge are the two main processes resulting in the mass loss from Greenland and Antarctica. Ice streams, which are characterised by a river-like structure of localised high flow velocities, contribute most to solid ice discharge and thus play a crucial role regarding future sea level rise (e.g., Bamber et al., 2000; van den Broeke et al., 2009; Margold et al., 2015; IPCC, 2022). However, ice-stream dynamics, including the internal deformation, are insufficiently understood (IPCC, 2013; Nick et al., 2013; Stokes et al., 2016). Therefore, the physics of ice streams must be investigated further to enable better projections of global sea level rise. Large-scale ice-flow models usually ignore the mechanical anisotropy of ice (Winkelmann et al., 2011) or assume (scalar) enhancement factors to approximate the effects of anisotropy in the bulk behaviour (e.g., Russell-Head and Budd, 1979; Rathmann et al., 2022). As it is only possible to measure ice flow velocity on the surface, except for very few locations with long-term accessible boreholes, it is not directly observed how ice in an ice stream behaves in the deeper ice column. Thus, the relative contributions to fast ice flow from internal deformation and basal sliding can only be estimated by inverse modelling, relying on standard descriptions of the rheological behaviour of ice. It is further unclear how and where the horizontal movement over the bed translates into shearing over bed.

Internal deformation is a significant component of ice flow, and its relative impact depends on the basal conditions. However, direct observational data from within the ice volume, i.e. from a deep ice core, are scarce due to the high costs and effort involved. To study the internal deformation in an ice stream, physical properties, such as the microstructure and Crystallographic Preferred Orientations (CPO) of ice crystals (also called crystal-orientation fabric or, in short, fabric), are examined and improve our understanding of the rheological behaviour of ice. A better description of ice rheological behaviour can then be implemented in large-scale flow models to advance our understanding of ice dynamics. Modelling ice CPOs and respective deformation regimes has advanced over the recent decades, becoming a powerful tool for investigating the dynamic behaviour of ice at different scales (e.g., Montagnat et al., 2014b; Richards et al., 2023). However, objectives and implemented processes usually differ from small-scale to large-scale flow models (e.g., Azuma and Higashi, 1985; Alley, 1992; Piazolo et al., 2019; Lilien et al., 2021; Llorens et al., 2022; Rathmann and Lilien, 2022; Richards et al., 2023; Ranganathan and Minchew, 2024). Information on the anisotropy in ice streams could be deduced to a certain extent by geophysical remote sensing methods, such as seismic (Smith et al., 2017) and radar (Jordan et al., 2022; Zeising et al., 2023; Gerber et al., 2023; Nymand et al., 2024) measurements. The most detailed ground-truth data are required from ice cores to verify the results of these remote sensing data in addition to improving modelling approaches.

https://doi.org/10.5194/egusphere-2024-2653
Preprint. Discussion started: 1 October 2024

Accurate information on the ice anisotropy and microstructural properties, such as grain size, can be derived via polarisation microscopy measurements of the c-axes orientations on consecutive thin-section samples from deep ice-core drillings. Measurements have been established utilising automated fabric analysers, typically at depth intervals of 10 to 150 m (e.g., Wang et al., 2003; Montagnat et al., 2014a; Fitzpatrick et al., 2014; Weikusat et al., 2017; Voigt, 2017). So far, most deep ice cores have been drilled at locations with low ice flow velocities, such as ice domes or divides, to guarantee an undisturbed record of climate signals (e.g., Petit et al., 1999; Watanabe et al., 2003; EPICA Community Members, 2004). Thus, direct observations of ice-sheet CPOs and microstructure were focused on these regions. However, the need for data from more dynamic regions is evident. The investigation of microstructural processes influenced by crystallographic preferred orientation, such as strain localisation and shear layers (e.g., Bons and Jessell, 1999; Llorens et al., 2016a; de Riese et al., 2019), largely unexplored in ice, would further benefit from data at high spatial resolution on anisotropy and deformation in an ice stream.

To investigate ice-stream dynamics by direct observation from within the ice, the East Greenland Ice-core Project (EastGRIP, main drilling between 2016 and 2023) retrieved the first continuous deep ice core through the central part of an active ice stream, i.e., the Northeast Greenland Ice Stream (NEGIS) (Fig. 1) — Greenland's most significant ice stream draining 12% of the ice sheet into the ocean (Rignot and Mouginot, 2012). Jansen et al. (2024) showed that NEGIS was dynamic in the Holocene and has only been established in its current form 2000 years ago. Further, the hardness of NEGIS for along-flow extension and compression is higher in the ice stream centre than at the shear margins, potentially indicating that fast-flowing ice bodies near the coast are sensitive to external disturbances (Gerber et al., 2023). First microstructural data from EastGRIP have assisted in investigating the localisation of impurities in the ice microstructure (Stoll et al., 2021a, 2022; Bohleber et al., 2023; Stoll et al., 2023) further studying the complicated interplay between impurities and the ice microstructure in regards to deformation and ice viscosity (e.g., Jones and Glen, 1969; Paterson, 1991; Eichler et al., 2017; Stoll et al., 2021b), in reconstructing the original orientation of the drilled core (Westhoff et al., 2021), and in understanding the birefringent radar echo patterns caused by CPO (Gerber et al., 2023).

The objectives of this study are to analyse, for the first time, the CPO evolution with depth throughout a site in the central part of a several-kilometre-wide ice stream derived via thin-section measurements from a deep ice core supplemented by grain-size and electrical-conductivity data. Complete measurements of 0.55 m pieces, i.e. entire "bags", of the ice core every 5–15 m exceed the semi-continuous sampling established in prior deep ice-core studies. The high depth coverage allows for the analysis of small-scale changes, in addition to the dominant deformation regimes and mechanisms inside NEGIS. Here, we focus on the investigation of the large-scale (hundreds of m) and mesoscale (m) changes of CPO with depth and derive the second-order orientation tensor's eigenvalues to explore the evolution of CPO and ice anisotropy with depth. We further compare the CPO development to other ice cores from Greenland and Antarctica aiming to highlight the unique characteristics of ice streams by considering different dynamical settings.

https://doi.org/10.5194/egusphere-2024-2653
Preprint. Discussion started: 1 October 2024

2 Methods

2.1 The EastGRIP ice core

The EastGRIP deep drilling succeeded in retrieving the first continuous ice core through an active ice stream. The drilling site is located at 75°38.16' N and 35°59.35' W (Fig. 1a), 2708 m a.s.l (May 2024), roughly 10 km away from the shear margins of NEGIS (Fig. 1b and c), the most significant ice stream in Greenland in terms of ice transport towards the margin (Fahnestock et al., 1993). The surface ice flow velocity at EastGRIP is ~55 m/yr (Hvidberg et al., 2020), but the velocity, location and flow dynamics of NEGIS probably changed throughout the Holocene (Franke et al., 2022; Jansen et al., 2024). Upstream of EastGRIP, the surface velocity and width of NEGIS are lower while it widens into faster flow downstream of the drill site (Fig. 1a) (Hvidberg et al., 2020). The site is characterised by an ice thickness of approximately 2665 m and an annual mean surface temperature of -28.7°C (Vandecrux et al., 2023).

Drilling started in 2016 and was interrupted for the 2020 and 2021 seasons due to the COVID-19 pandemic. Drilling resumed in 2022, and bedrock, consisting of water-saturated fine-grained sediment, was reached in August 2023 at a depth of approximately 2665 m. The bubble lock-in depth at EastGRIP is between 58 and 61 m of depth (Westhoff et al., 2023). The ice temperature profile (Fig. A1) follows a classic evolution with depth reaching a steady temperature of around -32°C at 200 m. Temperature increases from 1200 m downwards reaching -10°C at roughly 2450 m. The final measurements at 2665 m just above bedrock show -2.47°C, which is slightly below the pressure melting point.

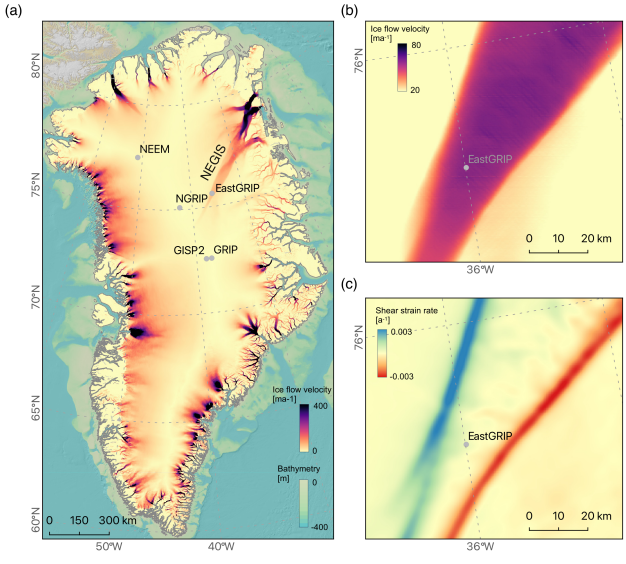

Figure 1. a) Overview of the surface ice flow velocity of Greenland (MEaSUREs ice velocity data set (Joughin et al., 2010a, b)). NEGIS and some deep ice coring sites are indicated. b) Detailed view of NEGIS surface ice flow velocity close to EastGRIP and the thereof c) derived shear strain rates.

https://doi.org/10.5194/egusphere-2024-2653
Preprint. Discussion started: 1 October 2024

2.2 Sample preparation

At the EastGRIP drill site, roughly every 5–15 m of depth, if possible, we cut 0.55 m long parallel to the core axis orientated ice core pieces into six sections of 9.2 x 7 cm ("vertical sections"). Unless indicated otherwise, the presented observations were carried out on vertical sections. This enables the continuous analysis of the stratigraphic variations in fabric with depth within 55 consecutive cm. Roughly every 100 m "horizontal sections" were taken from core volume samples of 10 cm length, providing snapshots of the ice crystal properties orthogonal to the core axis, thus enhancing the representation of three-dimensional crystals with two-dimensional measurements. In-situ core orientation, i.e. the azimuth angle, is not recorded directly during drilling as oriented drilling is still challenging. While this lack of orientation is not a constraint on obtaining results from the data analysis it may limit the interpretation. Only at depths where the methodological approach using visual stratigraphy (Westhoff et al., 2021) can be applied, the core azimuth may be reconstructed with reference to geographic coordinates.

For a combined analysis of microstructure and CPO, samples were cut into thick and thin sections with thicknesses of 130–160 mm and 0.3 mm, respectively. Remaining pieces were used for measurements of impurity localisation in the microstructure (e.g., Stoll et al., 2021a, 2022, 2023; Bohleber et al., 2023). The samples were frozen onto clean glass plates and microtomed with a Leica microtome sledge. A sharp blade enables micrometre-precise polishing via a micrometre screw, adjusting the distance between the blade and the stage. Each sample was left to sublimate under controlled conditions at the present temperature in the trench (-28 to -18°C) for the required time, usually ca. 1 hour, to increase the visibility of grain boundaries as they develop into sublimation grooves (e.g., Weikusat et al., 2009) and smooth the surface roughness affected by the polishing.

2.3 CPO and grain size measurements with the fabric analyser

We used the fabric analyser G50 manufactured by Russel-Head Instruments. The instrument automatically measures the CPO (Wilson et al., 2003) inside each thin section shortly after drilling during the field seasons where this was possible. We measured 1159 vertical and 66 horizontal sections over five field seasons (2017–2019, 2022–2023) from 165 continuous 55 cm ice-core sections. Due to varying ice-core quality, volume samples, and time constraints, the remaining measurements come from less continuous sections. The measurements cover an ice depth range within the ice stream from 111 m to 2663 m, which is almost the depth of the bedrock. Ice from the brittle zone (approximately 650–950 m (Westhoff et al., 2022)) was measured a year later to avoid samples breaking easily before relaxation. Between 2120 and 2417 m, no CPO data were measured so far due to the time delay inflicted by the COVID-19 pandemic-induced hiatus.

The fabric analyser uses polarised light microscopy to derive the orientation of the c-axis by using the birefringence of polarised light in optically anisotropic media. Thus, it is possible to measure one part of the full crystal orientation, i.e. the orientation of the main crystallographic axis, the c-axis. One standard measurement with a 20 μm resolution of a sample with dimensions of 9.2 x 7 cm takes roughly 45 minutes.

https://doi.org/10.5194/egusphere-2024-2653
Preprint. Discussion started: 1 October 2024

2.4 Fabric-analyser data processing

Raw image data were manually corrected to exclude artificial ice crystals that originate from the preparation process of the thin sections (Fig. A2). The corrected data are analysed with the software *cAxes* (Eichler, 2013). Threshold criteria regarding, for example, minimum crystal sizes (500 px equaling 0.2 mm^2), misorientation (1°), and sample quality, were applied. The derived data contain information about c-axis distribution, grain size, and the Woodcock parameter (Woodcock, 1977) - absolute or grain-weighted (Gagliardini et al., 2004). Grain area is calculated by transforming the pixels of single grains from the previously derived grain-boundary network into mm^2 yielding more exact results than older techniques, such as measuring the longest grain diameter or only a certain percentage of the largest grains. We here display the most common parameters to enable an overview of the core regarding deformation regimes.

2.5 Eigenvalues and fabric patterns

To analyse the shape and strength of the measured fabric data, the eigenvalues of the second-order orientation tensor for each sample are calculated. The measured c-axis orientations in polar coordinates are converted into Cartesian coordinates followed by the determination of the orientation tensor via standard structural geology methods (Wallbrecher, 1986). The c-axes distribution can be displayed as an ellipsoid with the eigenvectors representing the three orthogonal unit vectors along its axes originating from the centre of the ellipsoid (Woodcock, 1977). The lengths of the axes are represented by the invariant eigenvalues (e_1, e_2, e_3), which are usually normalised (λ_1, λ_2, and λ_3). They obey the conditions $\lambda_1+\lambda_2+\lambda_3=1$ and $\lambda_1 \leq \lambda_2 \leq \lambda_3$. The dominant fabric type can be determined using the eigenvalues according to the following rules:

- random fabric: $\lambda_1 \approx \lambda_2 \approx \lambda_3$, shape of a sphere;
- single-maximum: $0 \leq \lambda_1 \approx \lambda_2 \leq \frac{1}{6}$ and $\frac{2}{3} \leq \lambda_3 \leq 1$, shape of a prolate ellipsoid;
- girdle fabric: $\lambda_1 < \lambda_2 \approx \lambda_3$, shape of an oblate ellipsoid.

However, eigenvalues are most useful for unimodal distributions due to their inability to differentiate between certain fabric types, e.g., a narrow girdle and a multimaxima distribution. Thus, additional data representation such as stereographic projections is required to evaluate more complex fabric patterns.

2.6 Dielectric profiling

Dielectric profiling (DEP) enables the fast and non-destructive scanning of the electric conductivity and permittivity before cutting and processing the core further. At EastGRIP, DEP was performed on-site shortly after drilling with the device introduced by Wilhelms et al. (1998) to quickly locate positions of volcanic events and changes in chemical constituents. Conductivity in ice is mainly impacted by the acidity and the salt and ammonia concentrations (Moore et al., 1992). A detailed description of the instrument and the established procedure at EastGRIP can be found in Mojtabavi et al. (2020). We present DEP data of the deepest 260 m to enable a rough estimate of the depth-age relationship for deep ice, which has not been dated yet, providing context for interpreting the present microstructure and c-axes orientations.

https://doi.org/10.5194/egusphere-2024-2653
Preprint. Discussion started: 1 October 2024

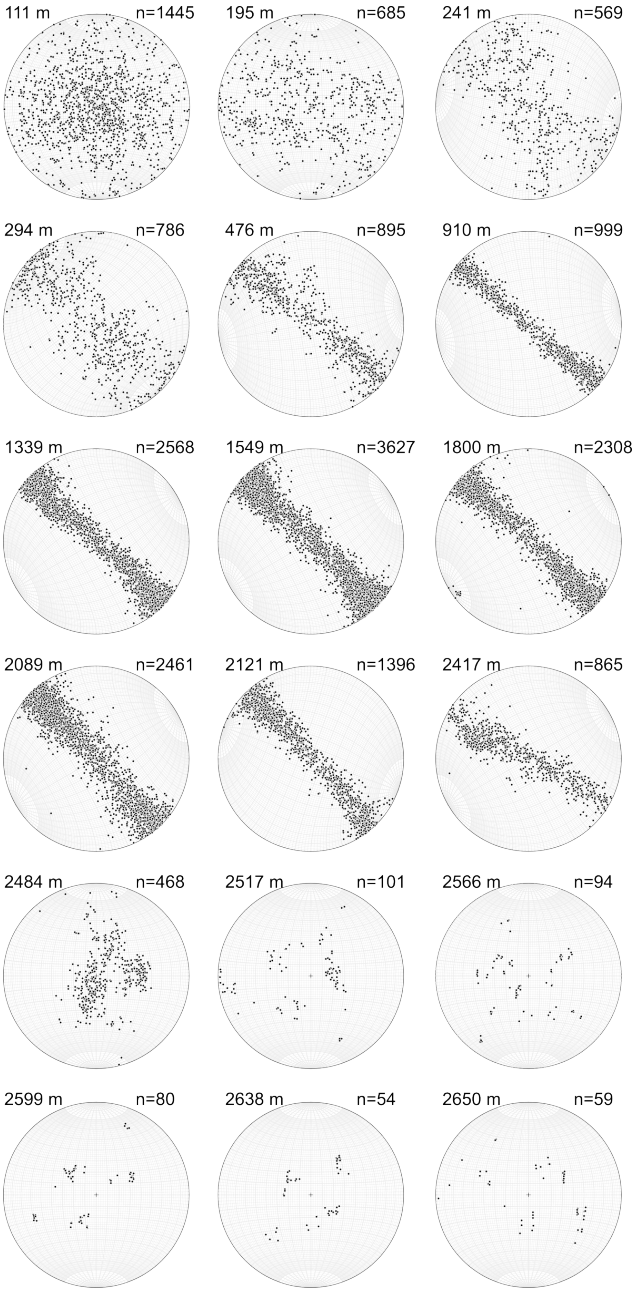

Figure 2. Representative selection of CPO patterns at EastGRIP displayed as equal-area lower hemisphere projections; depth and the number of analysed crystals (n) are indicated. The original azimuthal orientation is not preserved, but vertical girdles are rotated towards their estimated position (top represents geographical North) (Westhoff et al., 2021). All pole figures are provided in the supplements.

https://doi.org/10.5194/egusphere-2024-2653
Preprint. Discussion started: 1 October 2024

3 Results

3.1 CPO patterns in the EastGRIP ice core

The c-axis distributions, displayed as a selection of representative pole figures in Fig. 2 (all pole figures are provided in the supplements), reveal an evolution that has not been observed so far in a deep ice core. To enable the interpretation of the present CPO patterns, we must classify them and their respective depth regimes (Table 1). Most patterns are subject to gradual transitions and that the chosen depth regimes are inevitably subjective, approximations, and biased by the available data and can not be regarded as clearly defined.

The first 85 m, starting at an absolute depth of 111 m, show a broad single-maximum CPO. Between 196 and 294 m, especially around 240 m, a crossed girdle CPO occurs (Fig. 2 and 8), described for the first time in an ice core. This CPO occurs in two main types differing in the skeletal outline and the meeting point of the two girdles. Below 294 m, the crossed girdle CPO fully transitions into a broad, vertical girdle CPO. This CPO increases in strength, i.e. the girdle gets narrower, down to 1230 m. The vertical girdle sometimes shows horizontal maxima, which are fully established below 1394 m and occur down to 2500 m with varying strength. Between 2500–2663 m, the c-axes exhibit a multi-maxima CPO (Fig. 2 and 9). Most samples exhibit four to five maxima, which are centred around the vertical axis. Centimetre large crystals with amoeboid shapes and curved grain boundaries are abundant at this depth. However, the number of measured crystals (21–168) is usually still sufficient to identify CPO patterns. Only at the depth region 2608–2618 m crystals are several centimetre in length (see section 3.4), but combining data from six adjacent samples yields suitable statistics.

Table 1. Approximate depth regimes of the present CPO patterns at EastGRIP. In reality, CPO patterns are subject to gradual transitions and the specified depths are chosen for simplicity.

Approximate depth (m)	Age range b2k (ka)	CPO pattern
111–196	0.7–1.5	Broad Single-Maximum
196–294	1.5–2.3	Crossed Girdle
294–493	2.3–4.1	Crossed Girdle-Vertical Girdle Transition
493–1230	4.1–11.5	Vertical Girdle
1230–1394	11.5–15.3	Vertical Girdle with developing Horizontal Maxima
1394–2500	15.3–undefined	Vertical Girdle with Horizontal Maxima
2500–2663	undefined, possibly ~120	Multi-maxima

b2k: before 2000 CE after Mojtabavi et al. (2020) and Gerber et al. (2021).

3.2 Eigenvalue evolution with depth

We show the eigenvalue evolution as values per 9.2 x 7 cm thin section between 111 and 2663 m of depth. Fig. 3 displays it as a ternary diagram with the end-members random, point, and girdle CPO (e.g., Vollmer, 1990; Llorens et al., 2016b). For

https://doi.org/10.5194/egusphere-2024-2653
Preprint. Discussion started: 1 October 2024

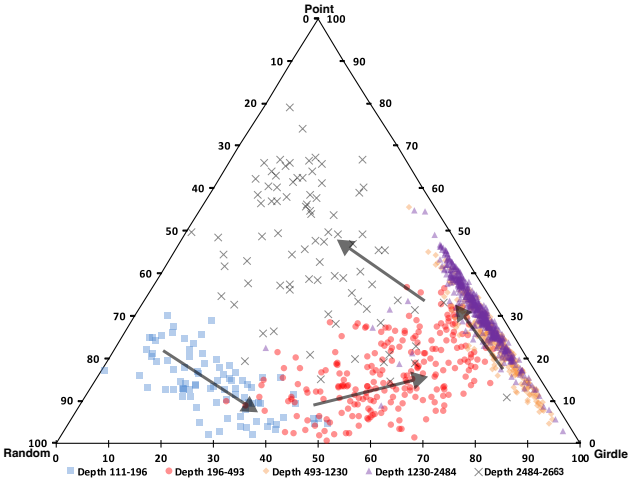

Figure 3. Ternary diagram displaying the CPO symmetry as the proportion of random, point, and girdle components of the measured c-axes (0001) means. Every marker represents one vertical thin section. Arrows display the evolution with depth.

EastGRIP, this shows the change in CPO with depth transforming from random with a point component to a strong girdle. Close to bedrock, it develops towards somewhere between point and random representing multi-maxima CPOs .

The classic representation of the three eigenvalues with depth is shown in Fig. 4a. Between 111 and 500 m, λ_1 decreases constantly and stays close to 0 until a depth of 2400 m. Values for λ_2 and λ_3 start around 0.25 and 0.5 at 111 m, respectively, developing quickly towards each other. At a depth of 250 m, these eigenvalues meet at 0.4. Until 900 m, λ_2 decreases slightly to around 0.35; it increases again until 1360 m, followed by a decrease and slow increase until 2100 m. λ_3 behaves opposite to λ_2 and oscillates around 0.65 until 900 m. λ_3 is at around 0.6 until 1200 m and increases slightly towards 1714 m, followed by a decrease until 2100 m. At a depth of 2400 m, λ_1 starts to increase up to 0.2, which is reflected in a decrease of λ_2 to minimum values of 0.15. Below 2550 m, λ_1 and λ_2 eigenvalues decrease due to an increase of λ_3 towards 0.8 close to bedrock. The variability of the eigenvalues is much greater at this depth than in shallower ice.

A wavy eigenvalue pattern of the two greater eigenvalues occurs from 550 m downwards (Fig. 4a). λ_2 and λ_3 display a repeated convergence and divergence with wavelengths ranging from dozens to hundreds of meters of depth. The amplitude of this wavy pattern is usually between 0.1–0.2. Both eigenvalues reach similar values at 650, 720, 930, 1110, 1370, and 1895 m.

The Woodcock parameter (Fig. 4b) lies in the interval 0–1 and 1–∞ for girdle and unimodal CPOs, respectively. In EastGRIP, the Woodcock parameter fluctuates between 1 and 6.2 in the shallowest analysed 70 m and decreases with depth. Between 180 and 2480 m, it is below 0.5. We detect slightly greater values between 228 and 250 m of depth. Below 2400 m, the Woodcock parameter increases and is often greater than 1. It sometimes exceeds 5 below 2483 m, correlating with the multi-maxima CPO. We excluded one outlier of 20.5 at 135.5 m in Fig. 4b, which is probably a measurement artefact.

https://doi.org/10.5194/egusphere-2024-2653
Preprint. Discussion started: 1 October 2024

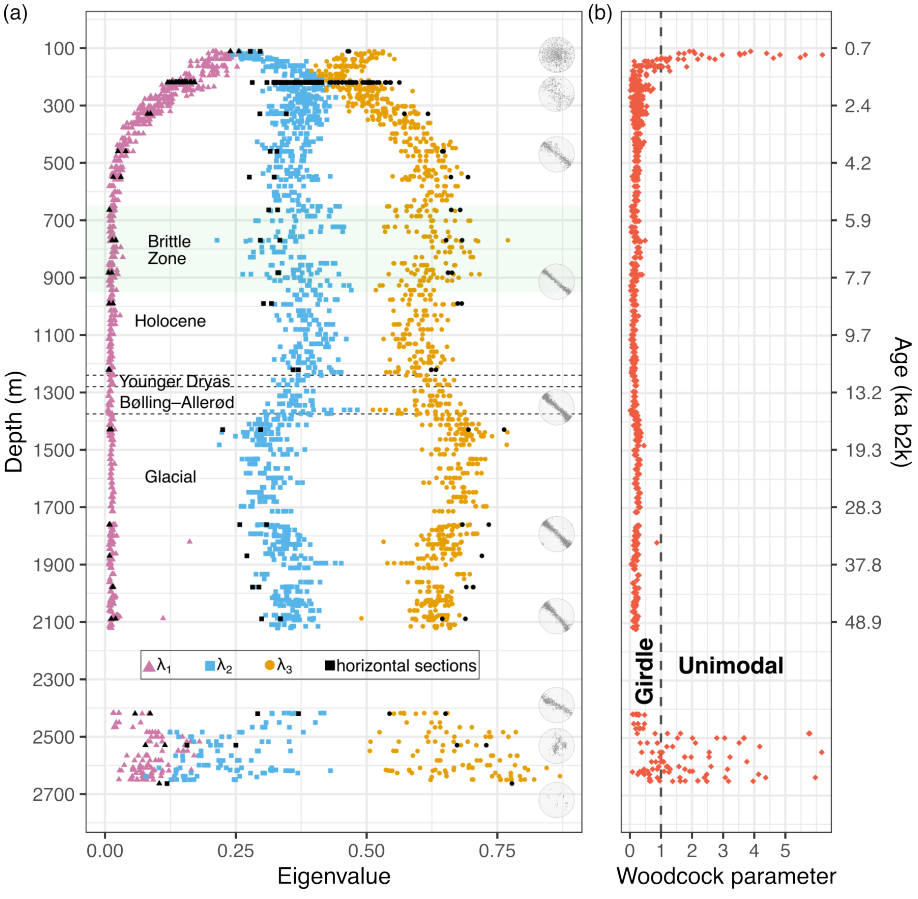

Figure 4. a) Orientation tensor eigenvalues of thin sections (9.2 x 7 cm) as derived by the fabric analyser and representative CPOs. Coloured eigenvalues are from vertical sections orientated parallel to the core axis; black symbols represent horizontal sections perpendicular to the core axis. Brittle zone (Westhoff et al., 2022) and climatic periods are indicated. b) Woodcock parameter, values above 1 represent unimodal CPOs; values below 1 indicate girdle CPOs. One outlier of 20.5 at 135.5 m of depth was excluded for better visibility. Shown values are grain-weighted. Age from Gerber et al. (2021), ice below 2118 m is not dated yet.

3.3 Grain size

The mean grain area, from hereon referred to as grain size, throughout the EastGRIP ice core is medium in Holocene ice, smaller but more consistent throughout the Last Glacial, and large close to bedrock (Fig. 5). In the upper 550 m, grain size reaches up to 10.3 mm^2. Grain size decreases to 3–6 mm^2 at 1000 m, increases slightly until 1100 m, and decreases to about 2–3 mm^2 at 1300 m. The grain size remains between 0.5 and 5.2 mm^2, mainly fluctuating around 1–2 mm^2, throughout the glacial until 2500 m. In the deepest ~150 m grain size strongly increases up to 280 mm^2 (Fig. 5).

The range of the mean grain size measured per thin section varies strongly throughout the core. The range is relatively large in the Holocene (Fig. 5), spanning up to 10 mm^2 between the smallest and largest mean values at similar depths. In the glacial,

https://doi.org/10.5194/egusphere-2024-2653
Preprint. Discussion started: 1 October 2024

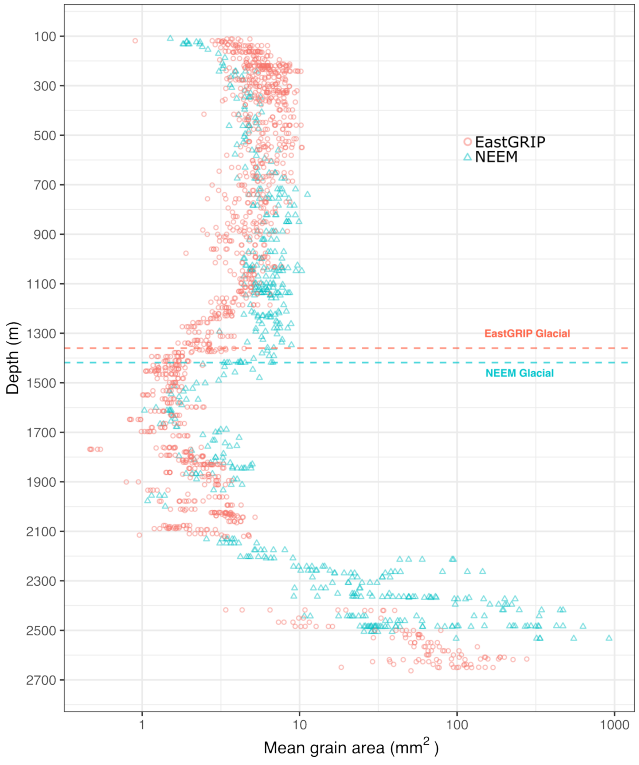

Figure 5. Comparison of the mean grain size between EastGRIP and NEEM (Montagnat et al., 2014a) derived by automated fabric analysers. Ice below the dotted lines is from the Last Glacial.

the variability is smaller, i.e. between 0.5 and 5 mm^2. At a depth of 2618 m, we recognised a large variability between adjacent samples (Fig. 6b).

3.4 Preliminary EastGRIP age estimate based on physical properties data

The DEP profile in Fig. 6a shows a distinct pattern, including some Greenland Interstadials and the Eemian-Glacial transition, following largely the North Greenland Ice Core Project (NGRIP) electrical conductivity measurement (ECM) profile (Rasmussen et al., 2013). EastGRIP DEP and microstructure data do not show indications of abrupt disturbances until a depth of 2618 m. At 2618.3 m, a sudden change in conductivity coincides with a change in crystal size and CPO over a few centimetres (Fig. 6b). Very large ice crystals (up to 7 cm in diameter) are followed by much smaller crystals resulting in a more blurred multi-maxima CPO (Fig. 6b).

https://doi.org/10.5194/egusphere-2024-2653
Preprint. Discussion started: 1 October 2024

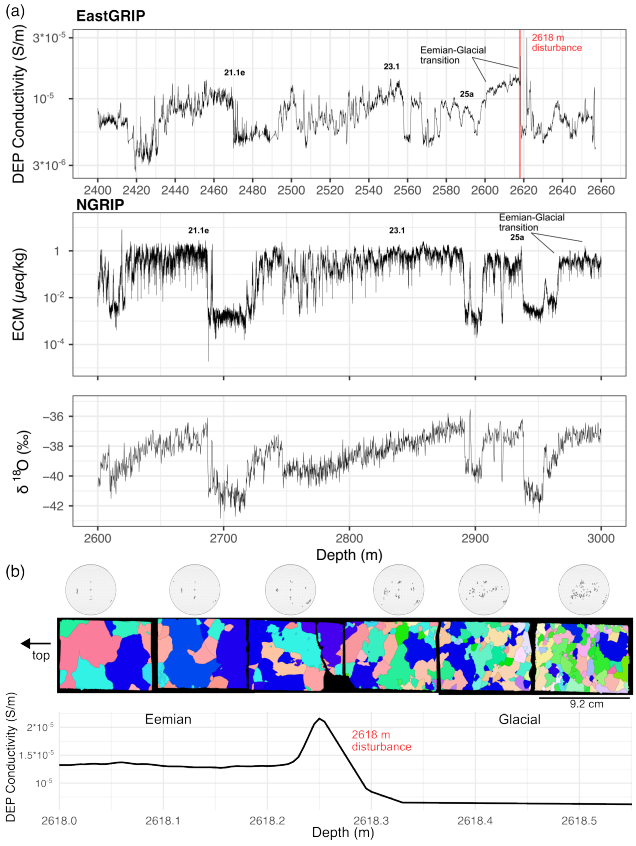

Figure 6. a) Conductivity data derived via DEP from the deepest 260 m compared to NGRIP ECM (Rasmussen et al., 2013) and oxygen isotopic ($\delta^{18}O$) (North Greenland Ice Core Project members, 2004) data. Greenland Interstadials are indicated after Rasmussen et al. (2014) enabling a first rough depth-age estimate. b) The strong conductivity change at 2618 m is also visible in the CPO (equal area lower hemisphere projections) and microstructure indicating a transition from Eemian ice (large crystals) to glacial ice (smaller crystals).

4 Discussion

4.1 Deformation regimes in NEGIS derived from CPOs

In the EastGRIP ice core, five different CPO patterns are present (Table 1). The two main processes affecting the CPO are 1) the rotation of c-axes due to deformation activated by the applied stresses (Llorens et al., 2022) and 2) the growth (positive and negative) of old grains or formation of new ice crystals with different orientations due to recrystallisation (Faria et al., 2014b). The first group of processes seems to dominate most of the ice column (Llorens et al., 2016b) even though indications of dynamic recrystallisation have been discovered throughout the core in a small number of selected samples (Stoll et al., 2021b). Fig. 3 shows the complex CPO evolution with depth at EastGRIP indicated by the variety of different proportion symmetries throughout the 2665 m. To disentangle this evolution, we derive information on the dominant deformation regimes from the

https://doi.org/10.5194/egusphere-2024-2653
Preprint. Discussion started: 1 October 2024

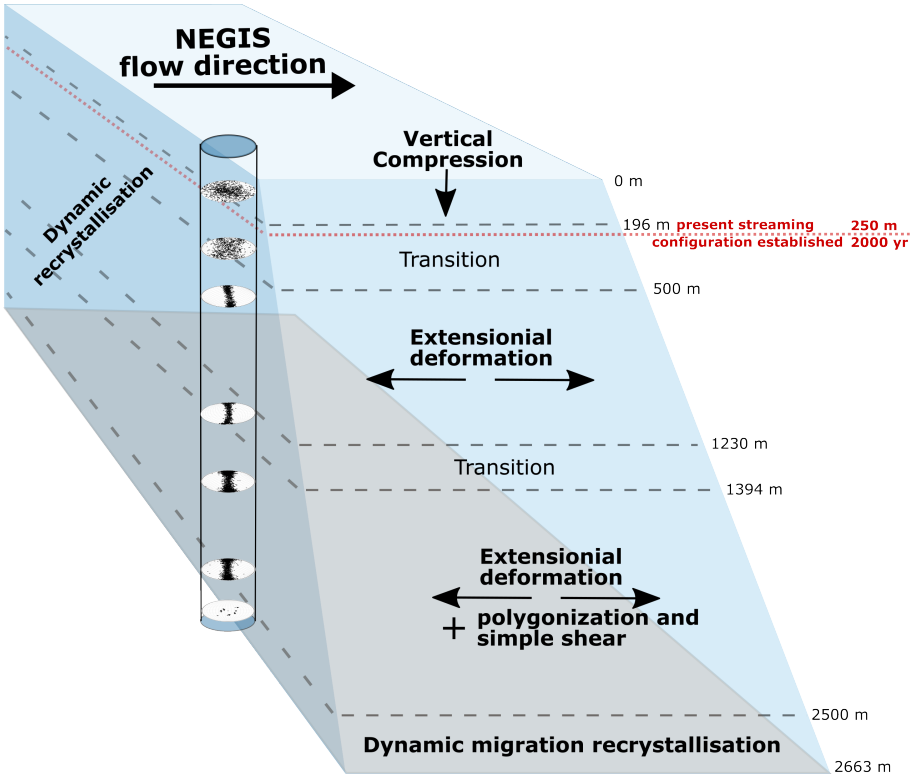

Figure 7. Sketch of NEGIS displaying the CPO patterns and the derived deformation regimes and recrystallisation processes. The red dotted line displays the depth when NEGIS was established in its current form (Jansen et al., 2024), everything below accumulated before today's ice stream conditions.

present CPO patterns as done for other deep ice cores (e.g., Kamb, 1972; Law et al., 1986; Alley, 1988; Thorsteinsson et al., 1997; Wang et al., 2002; Montagnat et al., 2014a; Faria et al., 2014b; Weikusat et al., 2017) and summarise them in Fig. 7.

4.1.1 Uniaxial compression in shallow ice

Between 111 and 196 m, we observe a broad single-maximum CPO. Here, most c-axes are loosely oriented towards the vertical axis. While a sequence of complex processes takes place in firn, including but not limited to densification, metamorphism and density-crossover phenomena (e.g., Freitag et al., 2004; Hörhold et al., 2012; Fujita et al., 2014, 2016; Montagnat et al., 2020), the initial CPO at the bottom of the firn is governed by vertically orientated uniaxial compression (coaxial dominated deformation) from overlying layers (e.g., Gow and Williamson, 1976; Thorsteinsson et al., 1997; Dahl-Jensen et al., 1997). Basal planes and their orthogonal c-axes are forced to rotate towards the axis of compression, which correlates with the ice core axis, enabling compression as displayed in deformation experiments (Azuma and Higashi, 1985). An additional horizontal extension component parallel to the ice stream direction is likely but indeterminable at this depth.

https://doi.org/10.5194/egusphere-2024-2653
Preprint. Discussion started: 1 October 2024

4.1.2 Hypotheses for the origin of the crossed girdle CPO

Crossed girdle CPOs have not been described before in ice, but has been in quartz and rocks containing quartz, such as shists or quartzites (e.g., Lister, 1974; Gross et al., 1978; Carreras and Garcia Celma, 1982; Law et al., 1986). Our crossed girdles are less distinct than examples described in the literature but differ from the broad single-maximum and vertical girdle above and below, respectively (Fig. 2 and 8). Crossed girdle CPOs were first categorised by Sander (1970) and later renamed into crossed girdle Type I and II (Lister, 1977). Type I is characterised by two girdles meeting at some distance from the intermediate strain axis and connected with a single girdle. In Type II, the two girdles meet at a point parallel to the intermediate strain axis (Schmid and Casey, 1986). Our studied CPOs vary between 1) both types and 2) different symmetry shapes regarding the intensity distribution and skeletal outline.

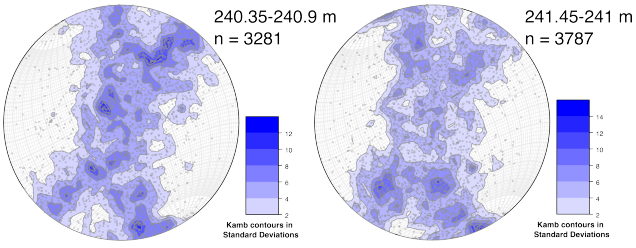

Figure 8. Kamb contours (Kamb, 1959) of crossed girdle CPOs compiled of six consecutive thin sections over 55 cm from two depths. Projections and annotation as in Fig. 2 excluding the rotation; note the slight differences in the legends.

For quartz, different explanations for the crossed girdle CPO exist. As quartz is a well-known analogue for ice (e.g., Wilson, 1979, 1981) due to similar rheological (hexagonal crystal structure, forming of polycrystalline aggregates, deformation via basal slip) and optical properties (Wilson and Russell-Head, 1979), it is assumed that both materials behave similarly during deformation, thus showing similar CPO patterns. Consequently, we derive the following possibilities for the crossed girdle:

- **Deformation history - approximate plane strain under pure shear (coaxial deformation) conditions** (Lister and Hobbs, 1980; Lister and Dornsiepen, 1982). An intermediate deformation regime between plane strain and flattening would result in a transitional CPO between a small circle girdle and a Type I crossed girdle (Law et al., 1986). The asymmetry of the crossed girdles could be related to different coaxial and non-coaxial strain paths (Lister and Hobbs, 1980) or increasing strain during simple shear deformation (Garcia Celma, 1983; Bouchez and Duval, 1982; Law et al., 1986).

- **Activation of non-basal slip systems** (Hirth and Lothe, 1982; Weertman and Weertman, 1992) as observed in other ice cores (e.g., Fukuda et al., 1987; Hondoh et al., 1990; Shearwood and Whitworth, 1991; Weikusat et al., 2011), resulting in the fast movement of short edge dislocation segments on non-basal planes providing mechanisms for accommodating heterogeneous strain and the multiplication of basal dislocations, such as Frank-Read sources (Frank and Read, 1950).

https://doi.org/10.5194/egusphere-2024-2653
Preprint. Discussion started: 1 October 2024

– **Overprinting of an older CPO during deformation** (Christie, 1963) caused by the establishment of NEGIS in its current form 2000 years ago (250 m) (Franke et al., 2022; Jansen et al., 2024).

– **Transition between broad single-maximum and vertical girdle** resulting in intermediate c-axis orientations as visible in the West Antarctic Ice Sheet (WAIS) Divide ice core at 1064 and 1264 m (Fig. 19 in Fitzpatrick et al. (2014)).

An in-depth investigation of the a-axes of EastGRIP samples between 200 and 250 m using Electron backscatter diffraction (EBSD) is required to test the hypotheses above but is beyond the scope of this overview study.

4.1.3 Uniaxial horizontal extension

From 294 m downwards, the crossed girdle changes into a broad vertical girdle CPO, which becomes more distinct with depth and is a fully established vertical girdle between 493 m and 1230 m. The vertical girdle is explained by uniaxial extension. During uniaxial longitudinal extension, as presumed for an ice stream, crystals rotate, and c-axes rotate away from the extension direction and, thus, the basal plane rotates towards the extensional direction. The vertical girdle plane in pole figures becomes oriented perpendicular to the axis of horizontal extension (Fujita et al., 1987; Alley, 1988; Thorsteinsson et al., 1997; Wang et al., 2002; Llorens et al., 2022). By combining visual stratigraphy and fabric data, Westhoff et al. (2021) demonstrated that the c-axes forming the girdle are orientated orthogonal to the ice flow present at the surface, proving that extension in the ice stream flow direction is the primary driver.

Vertical girdle CPOs were observed in the Antarctic ice cores Vostok, WAIS, EDML, and Mizuho (Fujita et al., 1987; Lipenkov et al., 1989; Fitzpatrick et al., 2014; Weikusat et al., 2017), and in the NGRIP ice core, Greenland (Wang et al., 2002). However, the impact of this fabric pattern on internal ice deformation is difficult to assess (Wang et al., 2002). In a vertical girdle, some crystals will be in a soft position, i.e. with c-axes 45° from the vertical compression axes. In contrast, other crystals are in a hard position against vertical compression.

4.1.4 Uniaxial horizontal extension complemented by rotation recrystallisation and a simple-shear component

The development from a vertical girdle to a vertical girdle with an asymmetrical two maxima CPO occurs between 1230 and 1394 m of depth, which is precisely the period of the transition from the Last Glacial to the Holocene (Mojtabavi et al., 2020) and is displayed in the broadening of the eigenvalue pattern (Fig. 4). At EastGRIP, the Holocene covers the upper 1240 m, followed by the Younger Dryas at 1240–1280 m, and the Bølling Allerød at 1280–1375 m (Mojtabavi et al., 2020). In contrast to NGRIP, the vertical girdle does not develop a maximum in the vertical direction parallel to the core axis (Wang et al., 2002), but maxima of varying strengths in the horizontal plane where one maximum is usually stronger (Fig. 2). Only glacial ice displays this CPO, which is thus likely related to the rheological differences between Holocene and glacial ice. Glacial ice has a higher number of insoluble particles, such as dust (e.g., Paterson, 1991; Stoll et al., 2021a, 2023), deposited during colder temperatures, and is characterised by smaller grains. Even though the detailed interplay between grain size and microstructure, impurities, and CPO remains ambiguous (Eichler et al., 2017, 2019; Stoll et al., 2021b), the differences between climate periods are unmistakable.

https://doi.org/10.5194/egusphere-2024-2653
Preprint. Discussion started: 1 October 2024

While the underlying CPO remains a vertical girdle due to longitudinal extension, glacial ice is characterised by a high rate of polygonization, also called rotation recrystallisation (e.g., Alley et al., 1995; Faria et al., 2014b; Ng and Jacka, 2014). It describes the splitting of grains into new grains with similar orientations by organising dislocations into low-angle subgrain boundaries. Thus, grain growth is balanced out creating a region of steady mean grain size and a stronger localisation of certain c-axis orientations. The horizontal maxima of the CPO could further be strengthened by an additional simple-shear component with a vertical shear plane as seen in a shear-margin core from ice stream B, West Antarctica (Jackson and Kamb, 1997) or the modelling work of Azuma (1994). Llorens et al. (2022) model the CPO development under ice-stream flow conditions first resulting in a vertical girdle due to uniaxial extension followed by horizontal point maxima with a girdle component due to simple shear. Additionally, Kamb (1972) showed the development of horizontal maxima CPOs with varying strengths in simple shear deformation experiments. If simple shear occurs as a secondary deformation regime, in addition to the longitudinal extension, a vertical girdle CPO with horizontal two-maxima could be the outcome. The comparably minor rheological differences within glacial ice, such as between stadials and interstadials or between cloudy bands and purer ice (Stoll et al., 2023), could explain the varying strength of the horizontal maxima as well as the wavy eigenvalue pattern (Fig. 4).

4.1.5 Dynamic recrystallisation close to bedrock

The deepest depth range (below 2500 m, temperature above -7.5°C) is characterised by multi-maxima CPO patterns of coarse-grained ice with interpenetrating grains of amoeboid shapes and curved grain boundaries (Fig. 2, 6, 9). Multi-maxima CPOs were observed in a few polar ice cores, such as the North Greenland Eemian Ice Drilling (NEEM) (Montagnat et al., 2014a), Byrd (Gow and Williamson, 1976), Cape Folger (Thwaites et al., 1984), and Law Dome (Zichu, 1985) and in temperate glaciers and ice caps (e.g., Rigsby, 1951; Hooke and Hudleston, 1980; Tison and Hubbard, 2000; Hellmann et al., 2021; Monz et al., 2021; Disbrow-Monz et al., 2024). Like EastGRIP, the present transitions to the multi-maxima CPO are often abrupt, accompanied by a change towards larger grain size, and occur close to bedrock where temperatures are typically high. Depending on the strain rate and temperature, different recrystallisation processes impact the microstructure (Faria et al., 2014b). The distinct fabric of clustered c-axes and the large interlocking grains indicate strong dynamic recrystallisation by grain-boundary migration (Gow and Williamson, 1976; Alley, 1988). The intensification of dynamic recrystallisation is fostered by the high temperature close to bedrock (above -10°C) (Fig. A1), high stresses, and large strains inflicted by potential basal shearing (Faria et al., 2014b). Another possibility is a regime of stagnant ice close to bedrock which would also result in large interlocked grains. Future borehole logging data will help in exploring this possibility.

In the EastGRIP ice core, dynamic recrystallisation has been observed from shallow depths downwards (Stoll et al., 2021a) similar to other ice cores (e.g., Alley, 1988; Weikusat et al., 2009; Kipfstuhl et al., 2009; Faria et al., 2014b). The two main types, according to Faria et al. (2014b), are rotation and migration recrystallisation. The latter, additionally called strain-induced boundary migration (SIBM), can be split up into nucleated migration recrystallisation (SIBM-N) and ordinary migration recrystallisation (SIBM-O) (Faria et al., 2014b). During SIBM-N, new grains nucleate in similar orientations as their parent grains, thus developing multi-maxima CPOs. Opposed to this, migrating grains during SIBM-O grow in size at the expenses of other grains and usually have similar orientations, resulting in single-maximum CPOs.

https://doi.org/10.5194/egusphere-2024-2653
Preprint. Discussion started: 1 October 2024

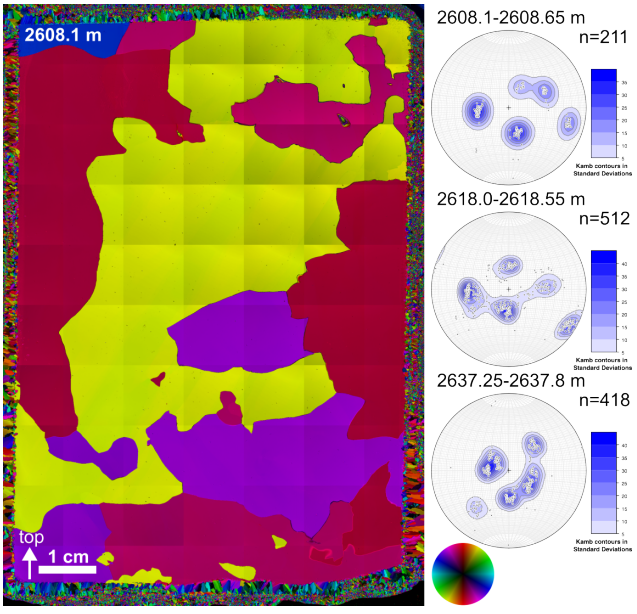

Figure 9. Example of the microstructure at 2608.1 m in c-axis orientation colour scale (see colour wheel on bottom right). Adjacent are three representative multi-maxima CPOs with Kamb contours (Kamb, 1959) compiled of six consecutive thin sections over 55 cm. The middle plot displays the transition from Eemian to glacial ice. Projections and annotation as in Fig. 2 excluding the rotation; note the slight differences in the legends.

The distinct microstructure in the form of large, amoeboid grains (Fig. 6b), the multi-maxima CPO pattern (Fig. 9), and the high ice temperature in the deepest 163 m (Fig. A1) enhancing grain-boundary mobility significantly indicate that SIBM-N is the dominant process in this depth regime. The multi-maxima CPO is not primarily a sampling issue caused by measuring grains multiple times as recently discussed (Monz et al., 2021; Disbrow-Monz et al., 2024). It persists when combining data from six vertically adjacent samples (Fig. 9), resulting in statistically relevant numbers of analysed crystals (≥ 211). A distinct study utilising high-resolution optical microstructure data will follow up on this.

4.2 Fast evolution of CPO compared to other ice cores

EastGRIP is the first deep ice core drilled through an ice stream. To investigate differences to traditional (palaeo-climatologically motivated), less dynamic ice coring sites, such as ice domes and divides, we compare the fabric evolution of EastGRIP with other ice cores with comparable large CPO data sets measured with automated c-axis fabric analysers (Fig. 10). The NEEM ice core was drilled on the Greenland ice divide only approximately 440 km northwest of EastGRIP, and was included due to this proximity and its similar age and temperature profiles (Montagnat et al., 2014a). EDML, at Kohnen Station, Antarctica, represents an ice divide with an extensional deformation regime and vertical girdle CPOs (Weikusat et al., 2017). Lastly, the South Pole Ice Core (SPICE), at the South Pole, Antarctica, represents flank flow and a relatively fast surface flow velocity of 10 m/yr (Casey et al., 2014; Voigt, 2017).

https://doi.org/10.5194/egusphere-2024-2653
Preprint. Discussion started: 1 October 2024

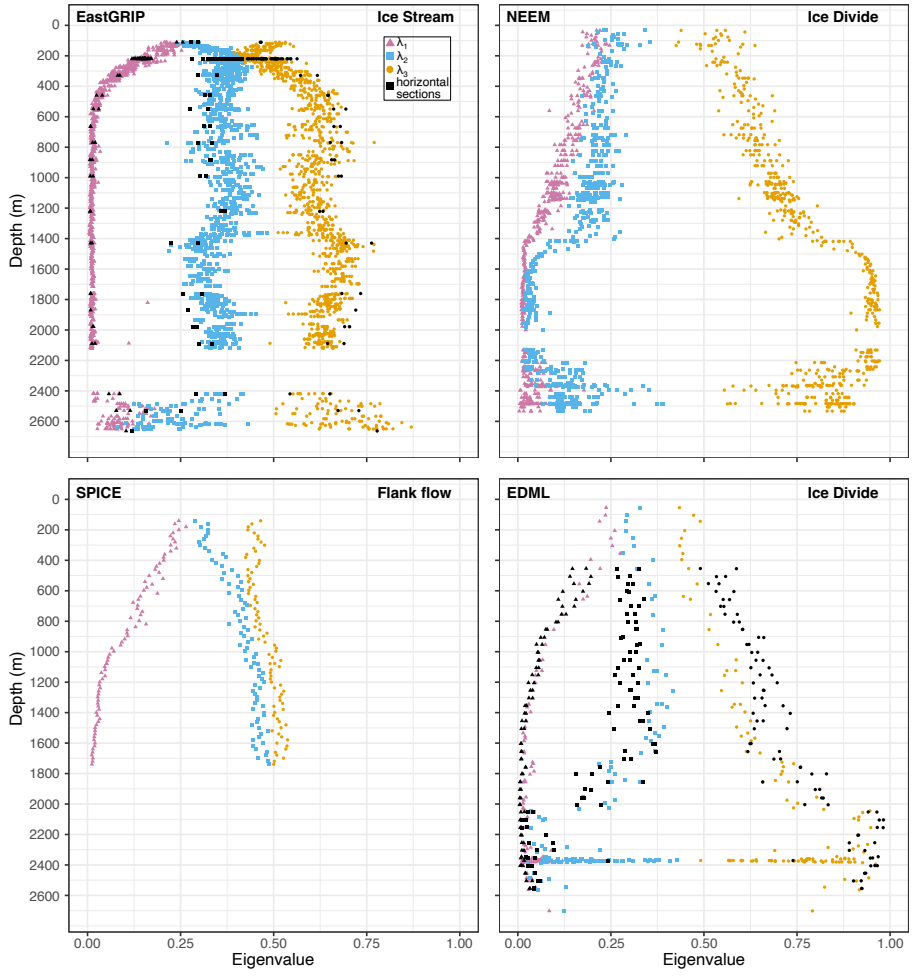

Figure 10. Comparison of the anisotropy evolution between EastGRIP, NEEM, EDML and SPICE via their eigenvalue development with depth (Montagnat et al., 2014a; Weikusat et al., 2017; Voigt, 2017). Note the differences between maximum values of λ_3 of EastGRIP and SPICE compared to NEEM and EDML. Annotations as in Fig. 4; all axes are formatted the same for better comparison.

The fast development of a strong anisotropy with depth is characterised by the rapid decrease of λ_1 at EastGRIP compared to the other cores (Fig. 10). λ_1 stabilises slightly above 0 at 500 m depth; similar values do not occur until depths greater than 1400 m, 1500 m and 1700 m at NEEM, EDML, and SPICE, respectively. Consequently, λ_3 at EastGRIP reaches higher values at shallower depth than in the other cores and remains between 0.5 and 0.8 until bedrock. In contrast, NEEM shows an abrupt increase in λ_3 at 1419 m, λ_3 of EDML gradually increases between 1600 and 2000 m whereas λ_3 of SPICE remains between 0.42 and 0.54. This comparison shows that the anisotropy development at EastGRIP is uniquely rapid. Thus, we show that assumptions valid for other, less dynamic locations cannot be applied for a location within NEGIS and likely other ice streams.

https://doi.org/10.5194/egusphere-2024-2653
Preprint. Discussion started: 1 October 2024

Even flank flow at SPICE differs strongly from the conditions at EastGRIP. The potential implications and consequences of this finding are discussed in section 4.5.1.

No other core exhibits wavy fluctuations in eigenvalues with depth in a manner similar to that at EastGRIP (Fig. 10). This difference could be partially an artefact from the much larger EastGRIP data set displaying more variation. The broader spread between 650 and 950 m correlates with the brittle zone at EastGRIP (Westhoff et al., 2022) and could be explained by the formation of small grains close to bubbles transforming into clathrates and natural variability. To explore this further, future studies on the single crystal scale and along particular depth regimes are needed at specific depths, such as the brittle zone, and for example, the depths around 1370 and 1895 m (Fig. 4).

4.3 Confirming the hypothesized vertical girdle CPO in ice streams

Our observational data enable us to confirm model assumptions about CPO patterns and deformation modes in active ice streams (e.g., Alley, 1988; Azuma, 1994; Llorens et al., 2022) enabling the transfer to other ice streams in Greenland and Antarctica. These studies assume that the c-axes of ice crystals rotate away from the axis of extension and thus produce a vertical girdle CPO with a potential horizontal maxima pattern. However, so far, only observations of the ice flow velocity on the surface of NEGIS indicate extensional behaviour. We can now confirm that within NEGIS, the most abundant deformation regime is longitudinal extension represented by a vertical girdle CPO.

4.4 Grain-size evolution in an ice stream

The examined grain-size trends with depth in EastGRIP are comparable to those in other Greenland deep ice cores (Faria et al., 2014a), such as the one observed in NEEM (Fig. 5) (Montagnat et al., 2014a). Both cores show medium grain sizes throughout the Holocene, followed by smaller values in the Last Glacial Period. Grains get significantly bigger roughly 200 m above bedrock due to 1) purer ice formed during the warmer conditions in the Eemian period and 2) warm ice (Fig. A1) caused by the proximity to bedrock and, thus, more geothermal heat. In the deepest part, the mean grain size at NEEM, also obtained with an automated fabric analyser and with partly larger samples, reaches up to 922 mm^2, while crystals at EastGRIP only reach about 280 mm^2.

The similar grain-size profiles between both cores, despite different CPOs and dynamic conditions (EastGRIP from an ice stream; NEEM from an ice divide) suggests no strong grain-size dependence of the dominating deformation regimes and large-scale ice dynamics here. Most NEEM samples are in a similar size range as EastGRIP, even close to bedrock. On smaller scales, the interplay between grain size, impurities, and CPO is more complex and remains difficult to disentangle (e.g., Paterson, 1991; Eichler et al., 2019; Stoll et al., 2021b). The more specific interpretation of grain size data will be presented in follow-up publications, as fabric analyser grain sizes (transmitting-light microscopy) are less accurate and generally coarser than reflected-light methods (Binder et al., 2013).

https://doi.org/10.5194/egusphere-2024-2653
Preprint. Discussion started: 1 October 2024

4.5 Implications

4.5.1 Relevance for ice sheets and ice-flow modelling

The presented data indicate that NEGIS, at the location of EastGRIP, mainly experiences extensional deformation along flow resulting in heterogeneous plug flow. Contrary to block flow this includes additional internal deformation components and heterogeneous strain and stress phenomena on different spatial scales indicated by the crossed girdle and vertical girdle with horizontal maxima CPOs. Despite their importance for ice-sheet and glacier mechanics, these microstructural features are usually overlooked in models (Faria et al., 2014b). We discuss the crossed girdle CPO for the first time in natural ice, and, to our knowledge, most ice fabric modelling has yet to produce similar CPOs. Thus, enhancing the bridging of different scales and approaches, as recently done by Richards et al. (2023); Ranganathan and Minchew (2024), is crucial.

A fundamental question arises regarding the upstream source and flow path of ice at various depths at EastGRIP, especially when considering the significance of the vertical fabric profile for ice sheet dynamics and the modeling of NEGIS. One key aspect is whether one assumes a constant velocity field in the past, where ice particles flow into NEGIS through the shear zone. This assumption is commonly used in modeling, mass-flux, and firn compaction studies (e.g., Holschuh et al., 2019; Gerber et al., 2021; Franke et al., 2021; Oraschewski and Grinsted, 2022; Gerber et al., 2023). Contrary to this assumption is the idea that shear zones in the upstream sector of NEGIS move with the ice stream over time and can cause the ice stream to either widen or narrow, reflecting a highly dynamic component in the development of NEGIS (Grinsted et al., 2022; Franke et al., 2022; Jansen et al., 2024). The different consequences arising from these two perspectives are highlighted in Jansen et al. (2024), where the sheared cylindrical folds are used as passive markers for ice flow. The fold deformation patterns at the shear margins do not align with the flow lines derived from the current ice flow velocity vectors, and instead indicate that ice remained inside the shear margins during the time of shearing.

Underlying this question is a long-standing fundamental debate on whether NEGIS, in its current form, represents a constant feature throughout the Holocene (Fahnestock et al., 2001) or whether NEGIS and similar ice streams are temporary phenomena that evolve with time and can switch on and off over a few thousand years (Franke et al., 2022; Jansen et al., 2024). While a detailed discussion of this topic is beyond the scope of this article, it is highly relevant for understanding the dynamic behavior of the Greenland Ice Sheet. It is clear, however, that the two theories - one positing an unchanging velocity field with ice flow through the shear zone and the other proposing a changing velocity field with moving shear zones—are fundamentally incompatible.

So far, we used the measured CPO data to establish the current deformation regimes at the EastGRIP site. However, there is a debate whether or not, and under which conditions, ice fabric can be used to reconstruct deformation and flow history (e.g., Lilien et al., 2021; Llorens et al., 2022). However, assuming that EastGRIP ice accumulated initially at the ice divide upstream of NEGIS before NEGIS was established, respective changes in flow and deformation history, i.e. changes in stress and strain conditions, could overprint or partly imprint the fabric (e.g., Lilien et al., 2021; Llorens et al., 2022). Llorens et al. (2022) show that the fabric at the onset of NEGIS would be preserved for a maximum of ~7 kyr while it would only remain for ~200 years at regions with higher strain, such as the shear margins.

https://doi.org/10.5194/egusphere-2024-2653
Preprint. Discussion started: 1 October 2024

Our EastGRIP data show no clear indications of overprinted CPO patterns, with the possible exception of the crossed girdle CPO around 250 m. This depth regime correlates with the timing of the establishment of NEGIS and its shear margins 2000 years ago (Fig. 7) (Jansen et al., 2024). Assuming that NEGIS in its current form is 2000 years old, as explained above, results in a unique change of deformation regimes inside the EastGRIP ice core over a short time around a depth of 250 m. Before either the establishment of NEGIS or the movement of EastGRIP ice into the ice stream, ice below 250 m of depth mainly experienced vertical compression and thus a different starting CPO than ice above 250 m, which mainly experienced a NEGIS-induced finite stretching along flow of approximately 175% and lateral shortening strain of approximately 67% in the last 2000 years (strain rates calculated with MEaSUREs ice velocity data set (Joughin et al., 2010a, b)). NEEM provides an estimate of the CPO and anisotropy profile at EastGRIP before NEGIS became established, which is represented by a weak and strong vertical c-axis maximum in shallow and kilometre-deep ice, respectively (Fig. 10). The potentially dynamic situation of NEGIS could explain the activation of different slip systems in EastGRIP ice, resulting in the crossed girdle CPO and a potential simple-shear component resulting in the vertical girdle with horizontal maxima. Further clarification could be obtained by analysing the borehole deformation via repeated borehole logging runs. So far, the derived CPO patterns seem to be reliable indicators of the ongoing ice flow while displaying remnants of the recent changes in ice dynamics of NEGIS (Jansen et al., 2024).

Our results show that in ice streams such as NEGIS, and likely others in Greenland and Antarctica, we cannot assume that the upper part of the ice column (upper two-thirds as assumed for ice divides (Dansgaard and Johnsen, 1969)) is dominated by vertical compression. Our observations reveal that specific stress- and strain regimes occur and must thus be represented better in ice-flow models. The novel insights from the EastGRIP ice core could help to take the next step towards more comprehensive ice flow and fabric modelling. Currently, we cannot derive if shearing takes place in the deepest layers due to the strong recrystallisation close to bedrock. Unfortunately, ice from the EastGRIP ice core does not contain strain markers as other rocks do, thus hampering the clear identification of changes in strain with microstructural methods. Repeated logging along the entire borehole is needed to detect and quantify these changes. However, long enough periods (often up to 12 months) between measurements are required to detect changes in the borehole geometry and, thus, potential shearing with certainty.

Our data, together with recent studies on the history and stability of NEGIS (Franke et al., 2022; Jansen et al., 2024), clearly display the complicated flow behaviour of NEGIS. These new insights imply that any changes regarding the flow behaviour of NEGIS, as the recently seen acceleration in several of its regions (Grinsted et al., 2022; Khan et al., 2022), could impact the entire thickness of the ice column resulting in higher solid ice discharge in the future if surface flow velocities keep increasing.

4.5.2 Potential for a record reaching back to the Eemian

Comparing EastGRIP DEP data to ECM data from the NGRIP ice core from Central Greenland shows a good correlation between both cores for their deepest parts (Fig. 6). We are thus able to present a rough first estimate of the approximate age of the EastGRIP ice core. Dating the entire EastGRIP core and processing the stable water isotope record are ongoing work. However, the large grain size in deep ice, and the correlating changes in CPO and conductivity, strongly indicate that the

https://doi.org/10.5194/egusphere-2024-2653
Preprint. Discussion started: 1 October 2024

EastGRIP ice core contains a record covering the climate transition from the Eemian into the Last Glacial Period similar to NEEM and NGRIP cores (NEEM community members, 2013; Rasmussen et al., 2014).

The sharp change in grain size correlating with a drop in electric conductivity at 2618.3 m (Fig. 6) indicate an abrupt transition from the Eemian towards ice from a so far unidentified glacial period below. This ice regime could thus be affected by shearing and folding but remains to be further characterised. However, EastGRIP has the potential to enable further investigation of the climate and the conditions of the Greenlandic Ice Sheet during the last interglacial.

5 Conclusions

The EastGRIP ice core enables the first overview of deformation regimes and CPO development throughout an ice stream while potentially reaching back to the Eemian. EastGRIP is characterised by five major deformation regimes accompanied by transition zones. The shallowest regime has undergone vertical compression from overlying layers yielding a broad single-maximum CPO. Below, we observe a crossed girdle CPO and provide hypotheses for its origin. The major regime is extensional deformation, which is indicated by a vertical girdle CPO. With depth, extensional deformation is accompanied by rotation recrystallisation and simple shear forming a vertical girdle with horizontal maxima. Close to bedrock high temperatures prevail resulting in dynamic migration recrystallisation visible in a multi-maximum CPO hindering the detection of the dominating deformation regime and the detection of potential basal shearing. We show that anisotropy develops considerably faster with depth than at less dynamic sites, such as ice divides and, even, ice flanks. The overall plug flow shows various small-scale variations, which require further research. Additional borehole logging is needed to decipher potential shearing above bedrock. By additionally discussing the grain size and ice temperature profile with depth, this study contributes towards a better understanding of the rheological behaviour and flow behaviour of ice streams while providing crucial data for improving future ice-flow models.

Appendix A

https://doi.org/10.5194/egusphere-2024-2653
Preprint. Discussion started: 1 October 2024

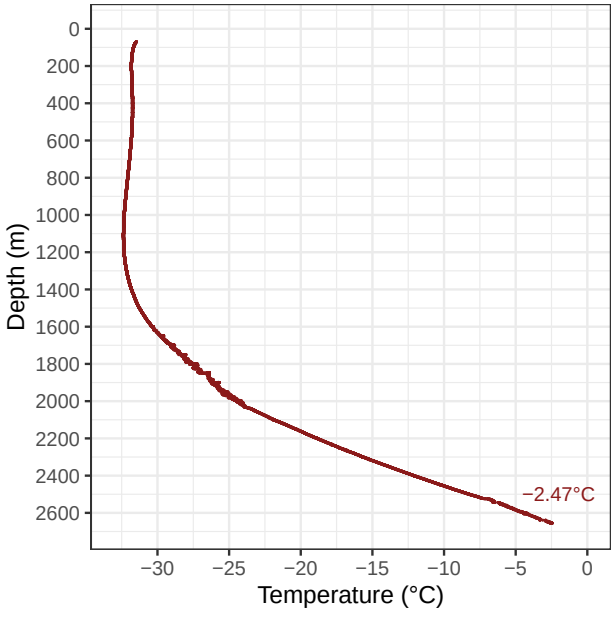

Figure A1. Temperature profile of the EastGRIP borehole derived by borehole logging on May 17 2024. Data from July 9, 2023, is shown below 2610 m because the logger could not go deeper in 2024 due to a glycol cavity at this depth. The deepest measurement shows a temperature of -2.47°C, which is slightly below the pressure melting point.

https://doi.org/10.5194/egusphere-2024-2653
Preprint. Discussion started: 1 October 2024

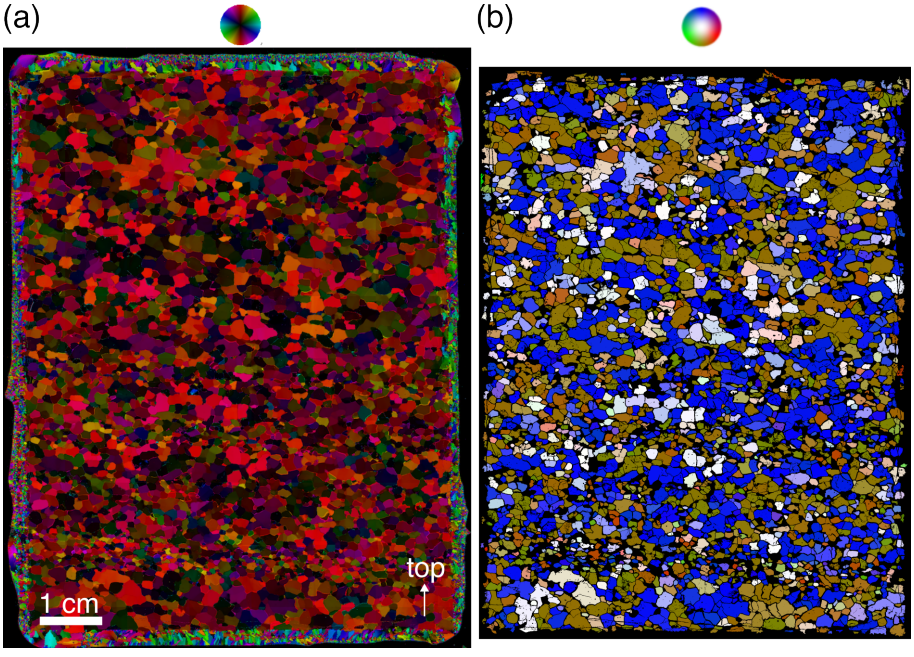

Figure A2. Measured fabric image and processed cAxes image from a depth of 1565.3 m. a) Original fabric image derived by the G50 fabric analyser. b) Image after processing with cAxes. The surrounding artificial ice, from glueing the sample to the plate, was digitally removed. The colours represent the orientation of the c-axis according to their respective colour wheels.

https://doi.org/10.5194/egusphere-2024-2653
Preprint. Discussion started: 1 October 2024

Data availability. Data will be made available via PANGAEA once the manuscript has been accepted.

Author contributions. The study was conceptualised by IW, DDJ, SK, JK, and NS. The manuscript was written by NS, IW, JK, KD, DJ with contributions from all authors. Fabric data were collected by NS, IW, JK, JE, DJ, JW, DW, TS, TH and processed and analysed by NS, JK, KD, IW, DJ with contributions from all authors. DEP data were collected by NS, DJ, JW, SK, and IW and processed by FW. Funding acquisition by IW, PB, FW, MD, and DDJ.

Competing interests. The authors declare that they have no conflict of interest.

Acknowledgements. We gratefully thank Steven Franke, Sebastian Hellmann, Pia Götz, Ina Kleitz, Wataru Shigeyama, Ernst-Jan Kuiper, Maddalena Bayer, Nicholas Rathmann, and Eliza Cook for their assistance in the sample preparation and measurement at EastGRIP. We thank Sonja Wahl, Florian Painer, Nils Hvidberg, Yannick Heiser, Nils F. Nymand, and Mikkel Lauritzen for contributing to the DEP data. We acknowledge Alexander Schlemmer for his technical support in setting up the environment for remote data processing. We further thank Steven Franke and Shuji Fujita for valuable input improving the quality of the manuscript. We thank the entire EastGRIP community for logistical assistance, ice core processing, and fruitful discussions. This work was carried out as part of the Helmholtz Junior Research group "The effect of deformation mechanisms for ice sheet dynamics" (VH-NG-802). Nicolas Stoll acknowledges additional funding from the Programma di Ricerche in Artico (PRA). EastGRIP is directed and organised by the Centre for Ice and Climate at the Niels Bohr Institute, University of Copenhagen. It is supported by funding agencies and institutions in Denmark (A. P. Møller Foundation, University of Copenhagen), USA (US National Science Foundation, Office of Polar Programs), Germany (Alfred Wegener Institute, Helmholtz Centre for Polar and Marine Research), Japan (National Institute of Polar Research and Arctic Challenge for Sustainability), Norway (University of Bergen and Trond Mohn Foundation), Switzerland (Swiss National Science Foundation), France (French Polar Institute Paul-Emile Victor, Institute for Geosciences and Environmental research), Canada (University of Manitoba) and China (Chinese Academy of Sciences and Beijing Normal University).

https://doi.org/10.5194/egusphere-2024-2653
Preprint. Discussion started: 1 October 2024

References

Alley, R. B.: Fabrics in polar ice sheets: Development and prediction, Science, 240, 493–495, https://doi.org/10.1126/science.240.4851.493, iSBN: 0036-8075 (Print) 0036-8075 (Linking), 1988.

Alley, R. B.: Flow-law hypotheses for ice-sheet modeling, Journal of Glaciology, 38, 1992.

Alley, R. B., Gow, A. J., and Meese, D. A.: Mapping c-axis fabrics to study physical processes in ice, Journal of Glaciology, 41, 197–203, https://doi.org/10.3189/S0022143000017895, 1995.

Azuma, N.: A flow law for anisotropic ice and its application to ice sheets, Earth and Planetary Science Letters, 128, 601–614, 1994.

Azuma, N. and Higashi, A.: Formation processes of ice fabric pattern in ice sheets, Annals of Glaciology, 6, 130–134, https://doi.org/10.1145/3209219.3209221, iSBN: 9781450355896, 1985.

Bamber, J. L., Vaughan, D. G., and Joughin, I.: Widespread complex flow in the interior of the antarctic ice sheet, Science, 287, 1248–1250, https://doi.org/10.1126/science.287.5456.1248, iSBN: 0036-8075, 2000.

Binder, T., Garbe, C., Wagenbach, D., Freitag, J., and Kipfstuhl, S.: Extraction and parametrization of grain boundary networks in glacier ice, using a dedicated method of automatic image analysis, Journal of Microscopy, 250, 130–141, https://doi.org/10.1111/jmi.12029, _eprint: https://onlinelibrary.wiley.com/doi/pdf/10.1111/jmi.12029, 2013.

Bohleber, P., Stoll, N., Rittner, M., Roman, M., Weikusat, I., and Barbante, C.: Geochemical Characterization of Insoluble Particle Clusters in Ice Cores Using Two-Dimensional Impurity Imaging, Geochemistry, Geophysics, Geosystems, 24, e2022GC010 595, https://doi.org/10.1029/2022GC010595, 2023.

Bons, P. D. and Jessell, M. W.: Micro-shear zones in experimentally deformed octachloropropane, Journal of Structural Geology, 21, 323–334, https://doi.org/10.1016/S0191-8141(98)90116-X, 1999.

Bouchez, J. L. and Duval, P.: The Fabric of Polycrystalline Ice Deformed in Simple Shear: Experiments in Torsion, Natural Deformation and Geometrical Interpretation, Textures and Microstructures, 5, 171–190, 1982.

Carreras, J. and Garcia Celma, A.: Quartz of C-Axis fabric variation at the margins of a shear zone developed in schists from Cap de Creus (Spain), Acta Geologica Hispanica, 17, 137–149, 1982.

Casey, K., Fudge, T., Neumann, T., Steig, E., Cavitte, M., and Blankenship, D.: The 1500 m South Pole ice core: recovering a 40 ka environmental record, Annals of Glaciology, 55, 137–146, https://doi.org/10.3189/2014AoG68A016, 2014.

Christie, J. M.: The Moine thrust zone in the Assynt region, northwest Scotland, University of California Press, https://cir.nii.ac.jp/crid/1130282270950398080, 1963.

Dahl-Jensen, D., Thorsteinsson, T., Alley, R., and Shoji, H.: Flow properties of the ice from the Greenland Ice Core Project ice core: The reason for folds?, Journal of Geophysical Research: Oceans, 102, 26 831–26 840, https://doi.org/10.1029/97JC01266, 1997.

Dansgaard, W. and Johnsen, S. J.: A Flow Model and a Time Scale for the Ice Core from Camp Century, Greenland, Journal of Glaciology, 8, 215–223, https://doi.org/10.3189/S0022143000031208, publisher: Cambridge University Press, 1969.

de Riese, T., Evans, L., Gomez-Rivas, E., Griera, A., Lebensohn, R. A., Llorens, M.-G., Ran, H., Sachau, T., Weikusat, I., and Bons, P. D.: Shear localisation in anisotropic, non-linear viscous materials that develop a CPO: A numerical study, Journal of Structural Geology, 124, 81–90, https://doi.org/10.1016/j.jsg.2019.03.006, 2019.

Disbrow-Monz, M. E., Hudleston, P. J., and Prior, D. J.: Multimaxima crystallographic fabrics (CPO) in warm, coarse-grained ice: New insights, Journal of Structural Geology, 182, 105 107, https://doi.org/10.1016/j.jsg.2024.105107, 2024.

https://doi.org/10.5194/egusphere-2024-2653
Preprint. Discussion started: 1 October 2024

Eichler, J.: C-axis analysis of the NEEM ice core: an approach based on digital image processing, Ph.D. thesis, Freie Universität Berlin, Berlin, issue: April, 2013.

Eichler, J., Kleitz, I., Bayer-Giraldi, M., Jansen, D., Kipfstuhl, S., Shigeyama, W., Weikusat, C., and Weikusat, I.: Location and distribution of micro-inclusions in the EDML and NEEM ice cores using optical microscopy and in situ Raman spectroscopy, Cryosphere, 11, 1075–1090, https://doi.org/10.5194/tc-11-1075-2017, 2017.

Eichler, J., Weikusat, C., Wegner, A., Twarloh, B., Behrens, M., Fischer, H., Hörhold, M., Jansen, D., Kipfstuhl, S., Ruth, U., Wilhelms, F., and Weikusat, I.: Impurity Analysis and Microstructure Along the Climatic Transition From MIS 6 Into 5e in the EDML Ice Core Using Cryo-Raman Microscopy, Frontiers in Earth Science, 7, 1–16, https://doi.org/10.3389/feart.2019.00020, 2019.

EPICA Community Members: Eight glacial cycles from an Antarctic ice core EPICA community members, Nature, 429, 623–628, iSBN: 0028-0836, 2004.

Fahnestock, M., Bindschadler, R., Kwok, R., and Jezek, K.: Greenland Ice Sheet Surface Properties and Ice Dynamics from ERS-1 SAR Imagery, Science, 262, 1530 LP – 1534, https://doi.org/10.1126/science.262.5139.1530, 1993.

Fahnestock, M., Abdalati, W., Joughin, I., Brozena, J., and Gogineni, P.: High Geothermal Heat Flow, Basal Melt, and the Origin of Rapid Ice Flow in Central Greenland, Science, 294, 2338 LP – 2342, https://doi.org/10.1126/science.1065370, 2001.

Faria, S. H., Weikusat, I., and Azuma, N.: The microstructure of polar ice. Part I: Highlights from ice core research, Journal of Structural Geology, 61, 2–20, https://doi.org/10.1016/j.jsg.2013.09.010, iSBN: 0191-8141, 2014a.

Faria, S. H., Weikusat, I., and Azuma, N.: The microstructure of polar ice. Part II: State of the art, Journal of Structural Geology, 61, 21–49, https://doi.org/10.1016/j.jsg.2013.11.003, 2014b.

Fitzpatrick, J. J., Voigt, D. E., Fegyveresi, J. M., Stevens, N. T., Spencer, M. K., Cole-Dai, J., Alley, R. B., Jardine, G. E., Cravens, E. D., Wilen, L. A., Fudge, T., and Mcconnell, J. R.: Physical properties of the WAIS Divide ice core, Journal of Glaciology, 60, 1181–1198, https://doi.org/10.3189/2014JoG14J100, 2014.

Frank, F. C. and Read, W. T.: Multiplication Processes for Slow Moving Dislocations, Physical Review, 79, 722–723, https://doi.org/10.1103/PhysRev.79.722, publisher: American Physical Society, 1950.

Franke, S., Jansen, D., Beyer, S., Neckel, N., Binder, T., Paden, J., and Eisen, O.: Complex Basal Conditions and Their Influence on Ice Flow at the Onset of the Northeast Greenland Ice Stream, Journal of Geophysical Research: Earth Surface, 126, e2020JF005 689, https://doi.org/10.1029/2020JF005689, 2021.

Franke, S., Bons, P. D., Westhoff, J., Weikusat, I., Binder, T., Streng, K., Steinhage, D., Helm, V., Eisen, O., Paden, J. D., Eagles, G., and Jansen, D.: Holocene ice-stream shutdown and drainage basin reconfiguration in northeast Greenland, Nature Geoscience, 15, 995–1001, https://doi.org/10.1038/s41561-022-01082-2, number: 12 Publisher: Nature Publishing Group, 2022.

Freitag, J., Wilhelms, F., and Kipfstuhl, S.: Microstructure-dependent densification of polar firn derived from X-ray microtomography, Journal of Glaciology, 50, 243–250, https://doi.org/10.3189/172756504781830123, 2004.

Fujita, S., Nakawo, M., and Shinji, M.: Orientation of the 700-m Mizuho core and its strain history, Proceedings of the NIPR Symposium on Polar Meteorology and Glaciology, 1, 122–131, https://cir.nii.ac.jp/crid/1571135651852389632, publisher: National Institute of Polar Research, 1987.

Fujita, S., Hirabayashi, M., Goto-Azuma, K., Dallmayr, R., Satow, K., Zheng, J., and Dahl-Jensen, D.: Densification of layered firn of the ice sheet at NEEM, Greenland, Journal of Glaciology, 60, 905–921, https://doi.org/10.3189/2014JoG14J006, 2014.

Fujita, S., Goto-Azuma, K., Hirabayashi, M., Hori, A., Iizuka, Y., Motizuki, Y., Motoyama, H., and Takahashi, K.: Densification of layered firn in the ice sheet at Dome Fuji, Antarctica, Journal of Glaciology, 62, 103–123, https://doi.org/10.1017/jog.2016.16, 2016.

https://doi.org/10.5194/egusphere-2024-2653
Preprint. Discussion started: 1 October 2024

Fukuda, A., Hondoh, T., and Higashi, A.: DISLOCATION MECHANISMS OF PLASTIC DEFORMATION OF ICE, Le Journal de Physique Colloques, 48, C1–163–C1–173, https://doi.org/10.1051/jphyscol:1987124, 1987.

Gagliardini, O., Durand, G., and Wang, Y.: Grain area as a statistical weight for polycrystal constituents, Journal of Glaciology, 50, 87–95, https://doi.org/10.3189/172756504781830349, num Pages: 87-95 Place: Cambridge, United Kingdom Publisher: Cambridge University Press, 2004.

Garcia Celma, A.: C-axis-and shape-fabrics in quartz-mylonites of Cap de Creus (Spain): their properties and development., Ph.D. thesis, Utrecht University, 1983.

Gerber, T. A., Hvidberg, C. S., Rasmussen, S. O., Franke, S., Sinnl, G., Grinsted, A., Jansen, D., and Dahl-Jensen, D.: Upstream flow effects revealed in the EastGRIP ice core using Monte Carlo inversion of a two-dimensional ice-flow model, The Cryosphere, 15, 3655–3679, https://doi.org/10.5194/tc-15-3655-2021, 2021.

Gerber, T. A., Lilien, D. A., Rathmann, N. M., Franke, S., Young, T. J., Valero-Delgado, F., Ershadi, M. R., Drews, R., Zeising, O., Humbert, A., Stoll, N., Weikusat, I., Grinsted, A., Hvidberg, C. S., Jansen, D., Miller, H., Helm, V., Steinhage, D., O'Neill, C., Paden, J., Gogineni, S. P., Dahl-Jensen, D., and Eisen, O.: Crystal orientation fabric anisotropy causes directional hardening of the Northeast Greenland Ice Stream, Nature Communications, 14, 2653, https://doi.org/10.1038/s41467-023-38139-8, number: 1 Publisher: Nature Publishing Group, 2023.

Gow, A. J. and Williamson, T.: Rheological implications of the internal structure and crystal fabrics of the West Antarctic ice sheet as revealed by deep core drilling at Byrd Station, GSA Bulletin, 87, 1665–1677, https://doi.org/10.1130/0016-7606(1976)87<1665:RIOTIS>2.0.CO;2, 1976.

Grinsted, A., Hvidberg, C. S., Lilien, D. A., Rathmann, N. M., Karlsson, N. B., Gerber, T., Kjær, H. A., Vallelonga, P., and Dahl-Jensen, D.: Accelerating ice flow at the onset of the Northeast Greenland Ice Stream, Nature Communications, 13, 5589, https://doi.org/10.1038/s41467-022-32999-2, 2022.

Gross, G. W., Hayslip, I. C., and Hoy, R. N.: Electrical donductivity and relaxation in ice crystals with known Impurity content, Journal of Glaciology, 21, 1978.

Hellmann, S., Kerch, J., Weikusat, I., Bauder, A., Grab, M., Jouvet, G., Schwikowski, M., and Maurer, H.: Crystallographic analysis of temperate ice on Rhonegletscher, Swiss Alps, The Cryosphere, 15, 677–694, https://doi.org/10.5194/tc-15-677-2021, 2021.

Hirth, J. P. and Lothe, J.: Theory of Dislocations, Krieger Publishing Company, Malabar, Florida, 1982.

Holschuh, N., Lilien, D. A., and Christianson, K.: Thermal Weakening, Convergent Flow, and Vertical Heat Transport in the Northeast Greenland Ice Stream Shear Margins, Geophysical Research Letters, 46, 8184–8193, https://doi.org/10.1029/2019GL083436, 2019.

Hondoh, T., Iwamatsu, H., and Mae, S.: Dislocation mobility for non-basal glide in ice measured by in situ X-ray topography, Philosophical Magazine A, 62, 89–102, https://doi.org/10.1080/01418619008244337, publisher: Taylor & Francis, 1990.

Hooke, R. L. and Hudleston, P. J.: Ice Fabrics in a Vertical Flow Plane, Barnes Ice Cap, Canada, Journal of Glaciology, 25, 195–214, https://doi.org/10.3189/S0022143000010443, 1980.

Hvidberg, C. S., Grinsted, A., Dahl-Jensen, D., Khan, S. A., Kusk, A., Andersen, J. K., Neckel, N., Solgaard, A., Karlsson, N. B., Kjær, H. A., and Vallelonga, P.: Surface velocity of the Northeast Greenland Ice Stream (NEGIS): assessment of interior velocities derived from satellite data by GPS, The Cryosphere, 14, 3487–3502, https://doi.org/10.5194/tc-14-3487-2020, publisher: Copernicus GmbH, 2020.

Hörhold, M. W., Laepple, T., Freitag, J., Bigler, M., Fischer, H., and Kipfstuhl, S.: On the impact of impurities on the densification of polar firn, Earth and Planetary Science Letters, 325-326, 93–99, https://doi.org/10.1016/j.epsl.2011.12.022, 2012.

https://doi.org/10.5194/egusphere-2024-2653
Preprint. Discussion started: 1 October 2024

IPCC: IPCC 13 Observations: Cryosphere, Climate Change 2013: The Physical Sci- ence Basis. Contribution of Working Group I to the Fifth Assessment Report of the Intergovernmental Panel on Climate Change, pp. 317–382, https://doi.org/10.1017/CBO9781107415324.012, iSBN: ISBN 978-1-107-66182-0, 2013.

IPCC: The Ocean and Cryosphere in a Changing Climate Special Report of the Intergovernmental Panel on Climate Change, Cambridge University Press, Cambridge, https://doi.org/10.1017/9781009157964.005, 2022.

Jackson, M. and Kamb, B.: The marginal shear stress of Ice Stream B, West Antarctica, Journal of Glaciology, 43, 415–426, https://doi.org/10.3189/S0022143000035000, 1997.

Jansen, D., Franke, S., Bauer, C. C., Binder, T., Dahl-Jensen, D., Eichler, J., Eisen, O., Hu, Y., Kerch, J., Llorens, M.-G., Miller, H., Neckel, N., Paden, J., de Riese, T., Sachau, T., Stoll, N., Weikusat, I., Wilhelms, F., Zhang, Y., and Bons, P. D.: Shear margins in upper half of Northeast Greenland Ice Stream were established two millennia ago, Nature Communications, 15, 1–12, https://doi.org/10.1038/s41467-024-45021-8, 2024.

Jones, S. J. and Glen, J. W.: The effect of dissolved impurities on the mechanical properties of ice crystals, Philosophical Magazine, 19, 13–24, https://doi.org/10.1080/14786436908217758, 1969.

Jordan, T. M., Martín, C., Brisbourne, A. M., Schroeder, D. M., and Smith, A. M.: Radar Characterization of Ice Crystal Orientation Fabric and Anisotropic Viscosity Within an Antarctic Ice Stream, Journal of Geophysical Research: Earth Surface, 127, e2022JF006 673, https://doi.org/10.1029/2022JF006673, 2022.

Joughin, I., Smith, B., Howat, I., and Scambos, T.: MEaSUREs Greenland Ice Sheet Velocity Map from InSAR Data, Version 1 [Data Set], 2010a.

Joughin, I., Smith, B. E., Howat, I. M., Scambos, T., and Moon, T.: Greenland flow variability from ice-sheet-wide velocity mapping, Journal of Glaciology, 56, 415–430, https://doi.org/10.3189/002214310792447734, publisher: Cambridge University Press, 2010b.

Kamb, B.: Experimental Recrystallization of Ice Under Stress, Flow and Fracture of Rocks, American Geophysical Union Geophysical Monograph, 16, 211–241, https://doi.org/10.1029/GM016p0211, 1972.

Kamb, W. B.: Ice petrofabric observations from Blue Glacier, Washington, in relation to theory and experiment, Journal of Geophysical Research (1896-1977), 64, 1891–1909, https://doi.org/10.1029/JZ064i011p01891, 1959.

Khan, S. A., Choi, Y., Morlighem, M., Rignot, E., Helm, V., Humbert, A., Mouginot, J., Millan, R., Kjær, K. H., and Bjørk, A. A.: Extensive inland thinning and speed-up of Northeast Greenland Ice Stream, Nature, pp. 1–6, https://doi.org/10.1038/s41586-022-05301-z, publisher: Nature Publishing Group, 2022.

Kipfstuhl, S., Faria, S. H., Azuma, N., Freitag, J., Hamann, I., Kaufmann, P., Miller, H., Weiler, K., and Wilhelms, F.: Evidence of dynamic recrystallization in polar firn, Journal of Geophysical Research: Solid Earth, 114, 1–10, https://doi.org/10.1029/2008JB005583, 2009.

Law, R. D., Casey, M., and Knipe, R. J.: Kinematic and tectonic significance of microstructures and crystallographic fabrics within quartz mylonites from the Assynt and Eriboll regions of the Moine thrust zone, NW Scotland, Transactions of the Royal Society of Edinburgh: Earth Sciences, 77, 99–125, https://doi.org/10.1017/S0263593300010774, iSBN: 1422-2868, 1986.

Lilien, D. A., Rathmann, N. M., Hvidberg, C. S., and Dahl-Jensen, D.: Modeling Ice-Crystal Fabric as a Proxy for Ice-Stream Stability, Journal of Geophysical Research: Earth Surface, 126, e2021JF006 306, https://doi.org/10.1029/2021JF006306, 2021.

Lipenkov, V. Y., Barkov, N. I., Duval, P., and Pimienta, P.: Crystalline Texture of the 2083 m Ice Core at Vostok Station, Antarctica, Journal of Glaciology, 35, 392–398, https://doi.org/10.3189/S0022143000009321, publisher: Cambridge University Press, 1989.

Lister, G. S.: The theory of deformation fabrics, Ph.D. thesis, Australian National University, 1974.

https://doi.org/10.5194/egusphere-2024-2653
Preprint. Discussion started: 1 October 2024

Lister, G. S.: Discussion: Crossed-girdle c-axis fabrics in quartzites plastically deformed by plane strain and progressive simple shear, Tectonophysics, 39, 51–54, https://doi.org/10.1016/0040-1951(77)90087-7, iSBN: 0040-1951, 1977.

Lister, G. S. and Dornsiepen, U. F.: Fabric transitions in the Saxony granulite terrain, Journal of Structural Geology, 4, 81–92, https://doi.org/10.1016/0191-8141(82)90009-8, iSBN: 0191-8141, 1982.

Lister, G. S. and Hobbs, B. E.: The simulation of fabric development during plastic deformation and its application to quartzite : the influence of detormation history, Journal of Structural Geology, 2, 355–370, 1980.

Llorens, M.-G., Griera, A., Bons, P. D., Lebensohn, R. A., Evans, L. A., Jansen, D., and Weikusat, I.: Full-field predictions of ice dynamic recrystallisation under simple shear conditions, Earth and Planetary Science Letters, 450, 233–242, https://doi.org/10.1016/j.epsl.2016.06.045, 2016a.

Llorens, M. G., Griera, A., Bons, P. D., Roessiger, J., Lebensohn, R., Evans, L., and Weikusat, I.: Dynamic recrystallisation of ice aggregates during co-axial viscoplastic deformation: A numerical approach, Journal of Glaciology, 62, 359–377, https://doi.org/10.1017/jog.2016.28, 2016b.

Llorens, M.-G., Griera, A., Bons, P. D., Weikusat, I., Prior, D. J., Gomez-Rivas, E., de Riese, T., Jimenez-Munt, I., García-Castellanos, D., and Lebensohn, R. A.: Can changes in deformation regimes be inferred from crystallographic preferred orientations in polar ice?, The Cryosphere, 16, 2009–2024, https://doi.org/10.5194/tc-16-2009-2022, publisher: Copernicus GmbH, 2022.

Margold, M., Stokes, C. R., and Clark, C. D.: Ice streams in the Laurentide Ice Sheet: Identification, characteristics and comparison to modern ice sheets, Earth-Science Reviews, 143, 117–146, https://doi.org/10.1016/j.earscirev.2015.01.011, publisher: Elsevier B.V. ISBN: 00128252, 2015.

Mojtabavi, S., Wilhelms, F., Cook, E., Davies, S. M., Sinnl, G., Skov Jensen, M., Dahl-Jensen, D., Svensson, A., Vinther, B. M., Kipfstuhl, S., Jones, G., Karlsson, N. B., Faria, S. H., Gkinis, V., Kjær, H. A., Erhardt, T., Berben, S. M. P., Nisancioglu, K. H., Koldtoft, I., and Rasmussen, S. O.: A first chronology for the East Greenland Ice-core Project (EGRIP) over the Holocene and last glacial termination, Climate of the Past, 16, 2359–2380, https://doi.org/10.5194/cp-16-2359-2020, 2020.

Montagnat, M., Azuma, N., Dahl-Jensen, D., Eichler, J., Fujita, S., Gillet-Chaulet, F., Kipfstuhl, S., Samyn, D., Svensson, A., and Weikusat, I.: Fabric along the NEEM ice core, Greenland, and its comparison with GRIP and NGRIP ice cores, Cryosphere, 8, 1129–1138, https://doi.org/10.5194/tc-8-1129-2014, 2014a.

Montagnat, M., Castelnau, O., Bons, P. D., Faria, S. H., Gagliardini, O., Gillet-Chaulet, F., Grennerat, F., Griera, A., Lebensohn, R. A., Moulinec, H., Roessiger, J., and Suquet, P.: Multiscale modeling of ice deformation behavior, Journal of Structural Geology, 61, 78–108, https://doi.org/10.1016/j.jsg.2013.05.002, 2014b.

Montagnat, M., Löwe, H., Calonne, N., Schneebeli, M., Matzl, M., and Jaggi, M.: On the Birth of Structural and Crystallographic Fabric Signals in Polar Snow: A Case Study From the EastGRIP Snowpack, Frontiers in Earth Science, 8, 1–23, https://doi.org/10.3389/feart.2020.00365, 2020.

Monz, M. E., Hudleston, P. J., Prior, D. J., Michels, Z., Fan, S., Negrini, M., Langhorne, P. J., and Qi, C.: Full crystallographic orientation (c and axes) of warm, coarse-grained ice in a shear-dominated setting: a case study, Storglaciären, Sweden, The Cryosphere, 15, 303–324, https://doi.org/10.5194/tc-15-303-2021, 2021.

Moore, J. C., Wolff, E. W., Clausen, H. B., and Hammer, C. U.: The chemical basis for the electrical stratigraphy of ice, Journal of Geophysical Research, 97, 1887–1896, https://doi.org/10.1029/91JB02750, 1992.

NEEM community members: Eemian interglacial reconstructed from a Greenland folded ice core, Nature, 493, 489–494, https://doi.org/10.1038/nature11789, publisher: Nature Publishing Group, 2013.

https://doi.org/10.5194/egusphere-2024-2653
Preprint. Discussion started: 1 October 2024

Ng, F. and Jacka, T. H.: A model of crystal-Size evolution in polar ice masses, Journal of Glaciology, 60, 463–477, https://doi.org/10.3189/2014JoG13J173, 2014.

Nick, F. M., Vieli, A., Andersen, M. L., Joughin, I., Payne, A., Edwards, T. L., Pattyn, F., and Van De Wal, R. S.: Future sea-level rise from Greenland's main outlet glaciers in a warming climate, Nature, 497, 235–238, https://doi.org/10.1038/nature12068, arXiv: NIHMS150003 Publisher: Nature Publishing Group ISBN: 1476-4687 (Electronic)\r0028-0836 (Linking), 2013.

North Greenland Ice Core Project members: High-resolution record of Northern Hemisphere climate extending into the last interglacial period, Nature, 431, 147–151, https://doi.org/10.1038/nature02805, publisher: Nature Publishing Group, 2004.

Nymand, N. F., Lilien, D. A., Gerber, T. A., Hvidberg, C. S., Steinhage, D., Gogineni, S. P., Taylor, D., and Dahl-Jensen, D.: Double reflections in novel polarized radar data reveal ice fabric in the North East Greenland Ice Stream (Preprint), Geophysical Research Letters, https://www.authorea.com/users/790985/articles/1061673-double-reflections-in-novel-polarized-radar-data-reveal-ice-fabric-in-the-north-east-greenland-ice-stream?commit=ec6923547174db143b47aaf78cedb27e0948457d, 2024.

Oraschewski, F. M. and Grinsted, A.: Modeling enhanced firn densification due to strain softening, The Cryosphere, 16, 2683–2700, https://doi.org/10.5194/tc-16-2683-2022, publisher: Copernicus GmbH, 2022.

Paterson, W. S. B.: Why ice-age ice is sometimes "soft", Cold Regions Science and Technology, 20, 75–98, 1991.

Petit, J. R., Jouzel, J., Raynaud, D., Barkov, N. I., Barnola, J.-M., Basile, I., Bender, M., Chappellaz, J., Davisk, M., Delaygue, G., Delmotte, M., Kotlyakov, V. M., Legrand, M., Lipenkov, V. Y., Lorius, C., Pépin, L., Ritz, C., Saltzmank, E., and Stievenard, M.: Climate and atmospheric history of the past 420,000 years from the Vostok ice core, Antarctica The recent completion of drilling at Vostok station in East, Nature, 399, 429–436, 1999.

Piazolo, S., Bons, P. D., Griera, A., Llorens, M.-G., Gomez-Rivas, E., Koehn, D., Wheeler, J., Gardner, R., Godinho, J. R. A., Evans, L., Lebensohn, R. A., and Jessell, M. W.: A review of numerical modelling of the dynamics of microstructural development in rocks and ice: past, present and future, Journal of Structural Geology, 125, 111–123, https://doi.org/10.1016/j.jsg.2018.05.025, 2019.

Ranganathan, M. and Minchew, B.: A modified viscous flow law for natural glacier ice: Scaling from laboratories to ice sheets, Proceedings of the National Academy of Sciences, 121, e2309788 121, https://doi.org/10.1073/pnas.2309788121, publisher: Proceedings of the National Academy of Sciences, 2024.

Rasmussen, S. O., Abbott, P. M., Blunier, T., Bourne, A. J., Brook, E., Buchardt, S. L., Buizert, C., Chappellaz, J., Clausen, H. B., Cook, E., Dahl-Jensen, D., Davies, S. M., Guillevic, M., Kipfstuhl, S., Laepple, T., Seierstad, I. K., Severinghaus, J. P., Steffensen, J. P., Stowasser, C., Svensson, A., Vallelonga, P., Vinther, B. M., Wilhelms, F., and Winstrup, M.: A first chronology for the North Greenland Eemian Ice Drilling (NEEM) ice core, Climate of the Past, 9, 2713–2730, https://doi.org/10.5194/cp-9-2713-2013, 2013.

Rasmussen, S. O., Bigler, M., Blockley, S. P., Blunier, T., Buchardt, S. L., Clausen, H. B., Cvijanovic, I., Dahl-Jensen, D., Johnsen, S. J., Fischer, H., Gkinis, V., Guillevic, M., Hoek, W. Z., Lowe, J. J., Pedro, J. B., Popp, T., Seierstad, I. K., Steffensen, J. P., Svensson, A. M., Vallelonga, P., Vinther, B. M., Walker, M. J. C., Wheatley, J. J., and Winstrup, M.: A stratigraphic framework for abrupt climatic changes during the Last Glacial period based on three synchronized Greenland ice-core records: refining and extending the INTIMATE event stratigraphy, Quaternary Science Reviews, 106, 14–28, https://doi.org/10.1016/j.quascirev.2014.09.007, 2014.

Rathmann, N. M. and Lilien, D. A.: Inferred basal friction and mass flux affected by crystal-orientation fabrics, Journal of Glaciology, 68, 236–252, https://doi.org/10.1017/jog.2021.88, publisher: Cambridge University Press, 2022.

https://doi.org/10.5194/egusphere-2024-2653
Preprint. Discussion started: 1 October 2024

Rathmann, N. M., Lilien, D. A., Grinsted, A., Gerber, T. A., Young, T. J., and Dahl-Jensen, D.: On the Limitations of Using Polarimetric Radar Sounding to Infer the Crystal Orientation Fabric of Ice Masses, Geophysical Research Letters, 49, e2021GL096 244, https://doi.org/10.1029/2021GL096244, 2022.

Richards, D. H., Pegler, S. S., Piazolo, S., Stoll, N., and Weikusat, I.: Bridging the Gap Between Experimental and Natural Fabrics: Modeling Ice Stream Fabric Evolution and its Comparison With Ice-Core Data, Journal of Geophysical Research: Solid Earth, 128, e2023JB027 245, https://doi.org/10.1029/2023JB027245, 2023.

Rignot, E. and Mouginot, J.: Ice flow in Greenland for the International Polar Year 2008–2009, Geophysical Research Letters, 39, https://doi.org/10.1029/2012GL051634, 2012.

Rigsby, G. P.: Crystal Fabric Studies on Emmons Glacier Mount Rainier, Washington, The Journal of Geology, 59, 590–598, https://doi.org/10.1086/625914, 1951.

Russell-Head, D. S. and Budd, W. F.: Ice-Sheet Flow Properties Derived from Bore-Hole Shear Measurements Combined With Ice-Core Studies, Journal of Glaciology, 24, 117–130, https://doi.org/10.3189/S0022143000014684, 1979.

Sander, N. R. B.: An Introduction to the Study of Geological Bodies, Geological Magazine, 107, 483–484, https://doi.org/10.1017/S001675680005768X, 1970.

Schmid, S. and Casey, M.: Complete fabric analysis of some commonly observed quartz C-axis patterns, Mineral and Rock Deformation, American Geophysical Union (AGU), https://doi.org/10.1029/GM036p0263, publication Title: Mineral and Rock Deformation: Laboratory Studies, AGU Geophysical Monographs Issue: 36 ISSN: 0875900623, 1986.

Shearwood, C. and Whitworth, R. W.: The velocity of dislocations in ice, Philosophical Magazine A, 64, 289–302, https://doi.org/10.1080/01418619108221186, 1991.

Smith, E. C., Baird, A. F., Kendall, J. M., Martín, C., White, R. S., Brisbourne, A. M., and Smith, A. M.: Ice fabric in an Antarctic ice stream interpreted from seismic anisotropy, Geophysical Research Letters, 44, 3710–3718, https://doi.org/10.1002/2016GL072093, 2017.

Stokes, C. R., Margold, M., Clark, C. D., and Tarasov, L.: Ice stream activity scaled to ice sheet volume during Laurentide Ice Sheet deglaciation, Nature, 530, 322–326, https://doi.org/10.1038/nature16947, publisher: Nature Publishing Group ISBN: 1476-4687 (Electronic)\r0028-0836 (Linking), 2016.

Stoll, N., Eichler, J., Hörhold, M., Erhardt, T., Jensen, C., and Weikusat, I.: Microstructure, micro-inclusions, and mineralogy along the EGRIP ice core – Part 1: Localisation of inclusions and deformation patterns, The Cryosphere, 15, 5717–5737, https://doi.org/10.5194/tc-15-5717-2021, 2021a.

Stoll, N., Eichler, J., Hörhold, M., Shigeyama, W., and Weikusat, I.: A Review of the Microstructural Location of Impurities and Their Impacts on Deformation, Frontiers in Earth Science, 8, https://doi.org/10.3389/feart.2020.615613, 2021b.

Stoll, N., Hörhold, M., Erhardt, T., Eichler, J., Jensen, C., and Weikusat, I.: Microstructure, micro-inclusions, and mineralogy along the EGRIP (East Greenland Ice Core Project) ice core – Part 2: Implications for palaeo-mineralogy, The Cryosphere, 16, 667–688, https://doi.org/10.5194/tc-16-667-2022, 2022.

Stoll, N., Westhoff, J., Bohleber, P., Svensson, A., Dahl-Jensen, D., Barbante, C., and Weikusat, I.: Chemical and visual characterisation of EGRIP glacial ice and cloudy bands within, The Cryosphere, 17, 2021–2043, https://doi.org/10.5194/tc-17-2021-2023, 2023.

Thorsteinsson, T., Kipfstuhl, J., and Miller, H.: Textures and fabrics in the GRIP ice core, Journal of Geophysical Research: Oceans, 102, 26 583–26 599, https://doi.org/10.1029/97JC00161, iSBN: 2156-2202, 1997.

Thwaites, R. J., Wilson, C. J. L., and McCray, A. P.: Relationship Between Bore-Hole Closure and Crystal Fabrics in Antarctic Ice Core from Cape Folger, Journal of Glaciology, 30, 171–179, https://doi.org/10.3189/S0022143000005906, 1984.

https://doi.org/10.5194/egusphere-2024-2653
Preprint. Discussion started: 1 October 2024

Tison, J.-L. and Hubbard, B.: Ice crystallographic evolution at a temperate glacier: Glacier de Tsanfleuron, Switzerland, Geological Society, London, Special Publications, 176, 23–38, https://doi.org/10.1144/GSL.SP.2000.176.01.03, publisher: The Geological Society of London, 2000.

van den Broeke, M., Bamber, J., Ettema, J., Rignot, E., Schrama, E., van de Berg, W. J., van Meijgaard, E., Velicogna, I., and Wouters, B.: Partitioning Recent Greenland Mass Loss, Science, 326, 984–986, https://doi.org/10.1126/science.1178176, 2009.

Vandecrux, B., Box, J. E., Ahlstrøm, A. P., Andersen, S. B., Bayou, N., Colgan, W. T., Cullen, N. J., Fausto, R. S., Haas-Artho, D., Heilig, A., Houtz, D. A., How, P., Iosifescu Enescu, I., Karlsson, N. B., Kurup Buchholz, R., Mankoff, K. D., McGrath, D., Molotch, N. P., Perren, B., Revheim, M. K., Rutishauser, A., Sampson, K., Schneebeli, M., Starkweather, S., Steffen, S., Weber, J., Wright, P. J., Zwally, H. J., and Steffen, K.: The historical Greenland Climate Network (GC-Net) curated and augmented level-1 dataset, Earth System Science Data, 15, 5467–5489, https://doi.org/10.5194/essd-15-5467-2023, publisher: Copernicus GmbH, 2023.

Voigt, D. E.: c-Axis Fabric of the South Pole Ice Core, SPC14, https://doi.org/10.15784/601057, 2017.

Vollmer, F. W.: An application of eigenvalue methods to structural domain analysis, GSA Bulletin, 102, 786–791, https://doi.org/10.1130/0016-7606(1990)102<0786:AAOEMT>2.3.CO;2, 1990.

Wallbrecher, E.: Tektonische und gefügeanalytische Arbeitsweisen: graphische, rechnerische und statistische Verfahren., Enke, Stuttgart, 1986.

Wang, Y., Thorsteinsson, T., Kipfstuhl, J., Miller, H., Dahl-Jensen, D., and Shoji, H.: A vertical girdle fabric in the NorthGRIP deep ice core, North Greenland, Annals of Glaciology, 35, 515–520, https://doi.org/10.3189/172756402781817301, iSBN: 0260-3055, 2002.

Wang, Y., Kipfstuhl, S., Azuma, N., Thorsteinsson, T., and Miller, H.: Ice-fabrics study in the upper 1500 m of the Dome C (East Antarctica) deep ice core, Annals of Glaciology, 37, 97–104, https://doi.org/10.3189/172756403781816031, publisher: Cambridge University Press, 2003.

Watanabe, O., Jouzel, J., Johnsen, S., Parrenin, F., Shoji, H., and Yoshida, N.: Homogeneous climate variability across East Antarctica over the past three glacial cycles, Nature, 422, 509–512, https://doi.org/10.1038/nature01525, 2003.

Weertman, J. and Weertman, J. R.: Elementary Dislocation Theory, Oxford University Press, Oxford, 1992.

Weikusat, I., Kipfstuhl, S., Faria, S. H., Azuma, N., and Miyamoto, A.: Subgrain boundaries and related microstructural features in EDML (Antarctica) deep ice core, Journal of Glaciology, 55, 461–472, https://doi.org/10.3189/002214309788816614, 2009.

Weikusat, I., Miyamoto, A., Faria, S. H., Kipfstuhl, S., Azuma, N., and Hondoh, T.: Subgrain boundaries in Antarctic ice quantified by X-ray Laue diffraction, Journal of Glaciology, 57, 111–120, https://doi.org/10.3189/002214311795306628, 2011.

Weikusat, I., Jansen, D., Binder, T., Eichler, J., Faria, S. H., Wilhelms, F., Kipfstuhl, S., Sheldon, S., Miller, H., Dahl-Jensen, D., and Kleiner, T.: Physical analysis of an Antarctic ice core—towards an integration of micro- and macrodynamics of polar ice, Philosophical Transactions of the Royal Society A: Mathematical, Physical and Engineering Sciences, 375, 20150 347, https://doi.org/10.1098/rsta.2015.0347, 2017.

Westhoff, J., Stoll, N., Franke, S., Weikusat, I., Bons, P., Kerch, J., Jansen, D., Kipfstuhl, S., and Dahl-Jensen, D.: A stratigraphy-based method for reconstructing ice core orientation, Annals of Glaciology, 62, 191–202, https://doi.org/10.1017/aog.2020.76, 2021.

Westhoff, J., Sinnl, G., Svensson, A., Freitag, J., Kjær, H. A., Vallelonga, P., Vinther, B., Kipfstuhl, S., Dahl-Jensen, D., and Weikusat, I.: Melt in the Greenland EastGRIP ice core reveals Holocene warm events, Climate of the Past, 18, 1011–1034, https://doi.org/10.5194/cp-18-1011-2022, 2022.

https://doi.org/10.5194/egusphere-2024-2653
Preprint. Discussion started: 1 October 2024

Westhoff, J., Freitag, J., Orsi, A., Martinerie, P., Weikusat, I., Dyonisius, M., Faïn, X., Fourteau, K., and Blunier, T.: Combining traditional and novel techniques to increase our understanding of the lock-in depth of atmospheric gases in polar ice cores - results from the EastGRIP region, https://doi.org/10.5194/egusphere-2023-1904, 2023.

Wilhelms, F., Kipfstuhl, J., Miller, H., Heinloth, K., and Firestone, J.: Precise dielectric profiling of ice cores: a new device with improved guarding and its theory, Journal of Glaciology, 44, 171–174, https://doi.org/10.3189/S002214300000246X, publisher: Cambridge University Press, 1998.

Wilson, C. J., Russell-Head, D. S., and Sim, H. M.: The application of an automated fabric analyzer system to the textural evolution of folded ice layers in shear zones, Annals of Glaciology, 37, 7–17, https://doi.org/10.3189/172756403781815401, 2003.

Wilson, C. J. L.: Boundary structures and grain shape in deformed multilayered polycrystalline ice, Tectonophysics, 57, T19–T25, https://doi.org/10.1016/0040-1951(79)90139-2, 1979.

Wilson, C. J. L.: Experimental folding and fabric development in multilayered ice, Tectonophysics, 78, 139–159, https://doi.org/10.1016/0040-1951(81)90011-1, iSBN: 0040-1951, 1981.

Wilson, C. J. L. and Russell-Head, D. S.: Experimental folding in ice and the resultant c-axis fabrics, Nature, 279, 49–51, https://doi.org/10.1038/279049a0, number: 5708, 1979.

Winkelmann, R., Martin, M. A., Haseloff, M., Albrecht, T., Bueler, E., Khroulev, C., and Levermann, A.: The Potsdam Parallel Ice Sheet Model (PISM-PIK) – Part 1: Model description, The Cryosphere, 5, 715–726, https://doi.org/10.5194/tc-5-715-2011, publisher: Copernicus GmbH, 2011.

Woodcock, N. H.: Specification of fabric shapes using an eigenvalue method, Geological Society of America Bulletin, 88, 1231–1236, 1977.

Zeising, O., Gerber, T. A., Eisen, O., Ershadi, M. R., Stoll, N., Weikusat, I., and Humbert, A.: Improved estimation of the bulk ice crystal fabric asymmetry from polarimetric phase co-registration, The Cryosphere, 17, 1097–1105, https://doi.org/10.5194/tc-17-1097-2023, publisher: Copernicus GmbH, 2023.

Zichu, X.: Ice Formation and Ice Structure on Law Dome, Antarctica, Annals of Glaciology, 6, 150–153, https://doi.org/10.3189/1985AoG6-1-150-153, 1985.